JOURNAL OF GEOPHYSICAL RESEARCH, VOL. 105, NO. B3, PAGES 5735–5770, MARCH 10, 2000

Active folding of fluvial terraces across the Siwaliks Hills, Himalayas of central Nepal

J. Lavé[1] and J. P. Avouac

Laboratoire de Géophysique, Commissariat à l'Energie Atomique, Bruyères-Le-Châtel, France

Abstract. We analyze geomorphic evidence of recent crustal deformation in the sub-Himalaya of central Nepal, south of the Kathmandu Basin. The Main Frontal Thrust fault (MFT), which marks the southern edge of the sub-Himalayan fold belt, is the only active structure in that area. Active fault bend folding at the MFT is quantified from structural geology and fluvial terraces along the Bagmati and Bakeya Rivers. Two major and two minor strath terraces are recognized and dated to be 9.2, 2.2, and 6.2, 3.7 calibrated (cal) kyr old, respectively. Rock uplift of up to 1.5 cm/yr is derived from river incision, accounting for sedimentation in the Gangetic plain and channel geometry changes. Rock uplift profiles are found to correlate with bedding dip angles, as expected in fault bend folding. It implies that thrusting along the MFT has absorbed 21 ± 1.5 mm/yr of N-S shortening on average over the Holocene period. The ±1.5 mm/yr defines the 68% confidence interval and accounts for uncertainties in age, elevation measurements, initial geometry of the deformed terraces, and seismic cycle. At the longitude of Kathmandu, localized thrusting along the Main Frontal Thrust fault must absorb most of the shortening across the Himalaya. By contrast, microseismicity and geodetic monitoring over the last decade suggest that interseismic strain is accumulating beneath the High Himalaya, 50–100 km north of the active fold zone, where the Main Himalayan Thrust (MHT) fault roots into a ductile décollement beneath southern Tibet. In the interseismic period the MHT is locked, and elastic deformation accumulates until being released by large ($M_w > 8$) earthquakes. These earthquakes break the MHT up to the near surface at the front of the Himalayan foothills and result in incremental activation of the MFT.

1. Introduction

The Himalaya is the most prominent and active intracontinental range in the world. Although the gross features of this active orogeny are now understood, the details of the seismotectonic behavior of the Himalaya are still poorly constrained. For example, the precise rate of crustal shortening across the range and the distribution of this deformation over the orogenic domain are mostly unknown. It is not clear whether the range thickens more or less homogeneously as a result of thrusting on many faults that are active simultaneously or whether deformation is localized on a major range-bounding thrust fault. We address these questions on the basis of a geomorphic analysis, complemented by geological investigations in central Nepal. Active deformation in the Himalaya region appears to be concentrated in the foothills [e.g., *Nakata*, 1989; *Yeats and Lillie*, 1991]. We thus focus on the Siwalik Hills along the piedmont and in particular on a 50-km-wide area south of the Kathmandu Basin (Figure 1).

Geomorphic evidence for active tectonics has been reported from several locations within the Siwalik Hills of Nepal [*Nakata*, 1972; *Delcaillau*, 1992; *Kimura*, 1995]. Our primary sources of evidence in the study area were warped and tilted fluvial terraces. Fluvial terraces are particularly useful features since they can provide information on rates of rock uplift (and hence rates of folding, if rock uplift can be related to folding) [e.g., *Rockwell et al*., 1984; *Molnar*, 1987; *Molnar et al*., 1994]. To derive rock uplift rate from dated fluvial terraces, it is generally assumed that the geometry and elevation of the river remain constant during downcutting. Rock uplift is equal to river incision, as measured from the elevation of terrace remnants above the modern river channel. However, a river can also incise due to climatically induced channel geometry and base level changes, so that local incision does not necessarily equal local tectonic uplift. It is generally considered that fluvial terraces forming a level at a continuously varying elevation above the modern river bed are isochronous [e.g., *Rockwell et al*., 1984; *Molnar et al*., 1994]. However, recent advances in geomorphology have shown that terraces can be time-transgressive [*Weldon*, 1986; *Bull*., 1991] and that the age control obtained from isolated samples collected in terrace overbank deposits might be significantly biased [*Merritts et al*., 1994; *Personius*, 1995]. With these limitations in mind, we have collected and analyzed our data to constrain as tightly as possible the terrace record of river incision and to derive tectonic uplift.

We first review some aspects of Himalayan tectonics and geology that are relevant to our study. We then focus on the Himalayan foothills of central Nepal, south of Kathmandu, starting with a structural and stratigraphic description of the Siwalik Fold Belt. Subsequently, we describe fluvial terraces that have been generated along two rivers, the Bagmati and Bakeya, which cut across the frontal fold belt. Tectonic uplift is retrieved from river incision, accounting for initial terrace geometry. To this end, we consider channel sinuosity changes as

[1]Now at Laboratoire de Géodynamique des Chaînes Alpines, Grenoble, France.

Paper number 1999JB900292.
0148-0227/00/1999JB900292$09.00

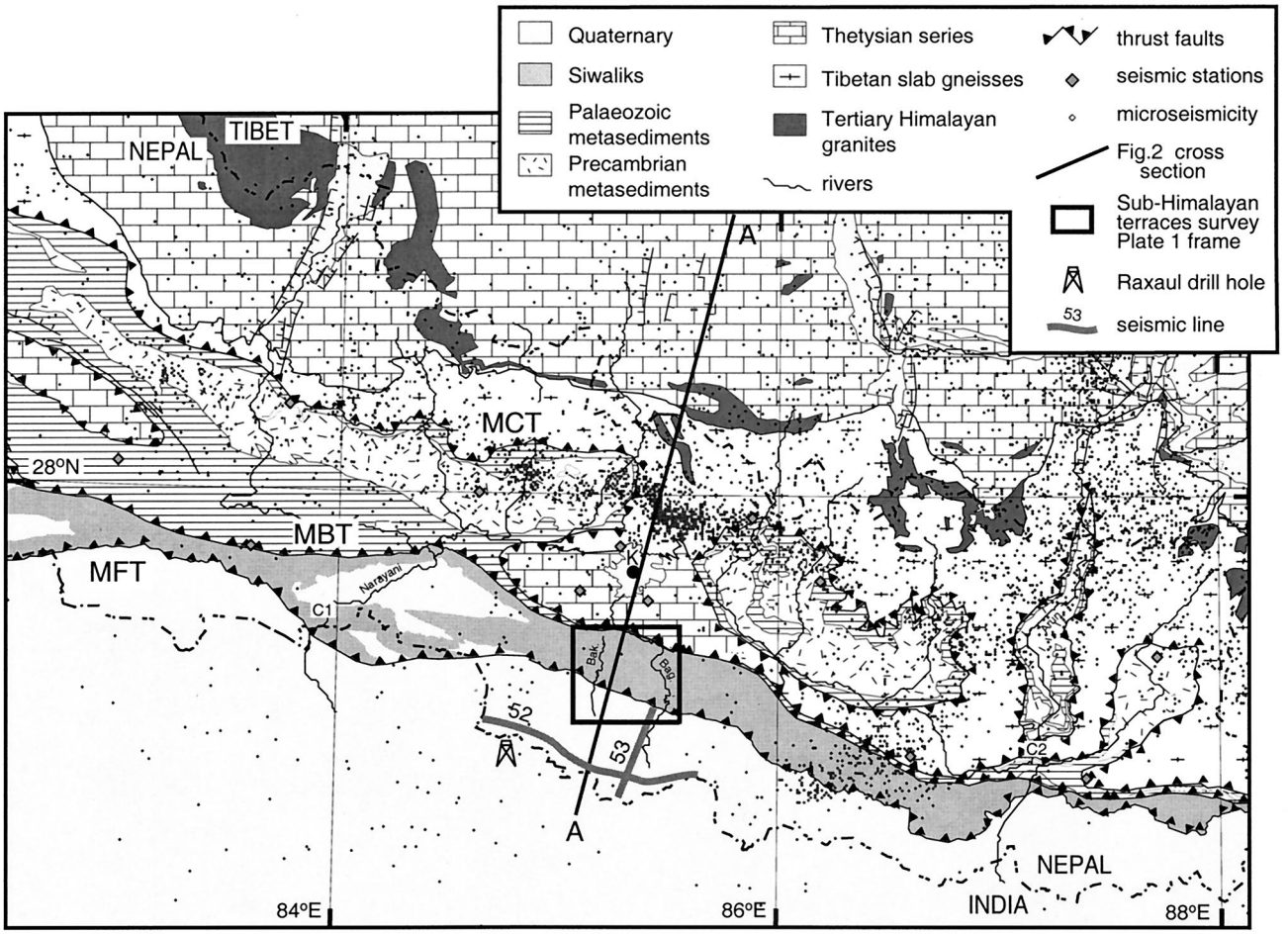

Figure 1. Geology and seismicity of Nepal. The geological map was modified from the Nepalese 1:50,000 geological map (courtesy of the Department of Mines and Geology (DMG)), *Schelling* [1992b], *Brunel* [1986], and *Stöcklin* [1980], and for the Tibetan part from *Gansser* [1964]. Microseismicity recorded between 1994 and 1996 [courtesy of the Seismological Laboratory, DMG) closely follows the front of the Higher Himalaya. Box indicates the present study area. The shaded lines are seismic lines 52 and 53 (courtesy of the Petroleum Project, DMG) interpreted in Figure 3.

well as base level changes due to sedimentation in the foreland. We relate the uplift profiles to a simple model of fold deformation, based on the descriptions of the structural geology, and thus derive the shortening rate across the Siwaliks Hills. In the last section, we discuss implications for Himalayan seismotectonics by linking these observations with other geological and geophysical information.

2. Geological Setting

2.1. General Background

About 50 Myr ago, India collided with the southern edge of Eurasia along the Indus Tsangpo Suture Zone (ITSZ) [e.g., *Molnar and Tapponnier*, 1975]. Subsequently, India and stable Eurasia continued to converge at a rate of ~5 cm/yr [*Patriat and Achache*, 1984]. A fraction of this convergence has been absorbed by crustal thickening of the northern margin of the Indian continent associated with the activation of several major thrust zones. The southern deformation front has migrated southward with the successive activation of the Kangmar Thrust, the Main central Thrust (MCT), and the Main Boundary Thrust (MBT) (Figures 1 and 2) [*Gansser*, 1964; *Le Fort*, 1986; *Brunel*, 1986; *Ratschbacher et al*., 1994]. The high-grade metamorphic units of the Higher Himalaya lie north of the MCT and medium-grade metamorphic rocks form the Lesser Himalaya between the MCT and the MBT [*Le Fort*, 1975, 1986; *Brunel*, 1986]. The sub-Himalaya consists of the Siwalik Hills which extend south of the MBT [*Hérail and Mascle*, 1980; *Mascle and Hérail*, 1982]. The Indo-Gangetic foredeep formed in front of the rising Himalayan range and trapped a fraction of the material eroded away from the areas of high relief. Several kilometers of Cenozoic molasse deposits (Murrees and Siwaliks Formations) have thus accumulated on the Precambrian Indian basement and were scraped off at the range front by continued overthrusting. The induced thin-skinned tectonics has led to the formation of the sub-Himalayan foothills that now mark the active deformation front, with the Main Frontal Thrust (MFT) lying at their southern edge [*Nakata*, 1989]. North of the MFT, the décollement of the Indian basement is thought to extend as a flat beneath the Lesser Himalaya and to form a steeper ramp at the front of the High Himalaya [*Schelling and Arita*, 1991; *Schelling*, 1992b; *Pandey et al*., 1995] (Figure 2).

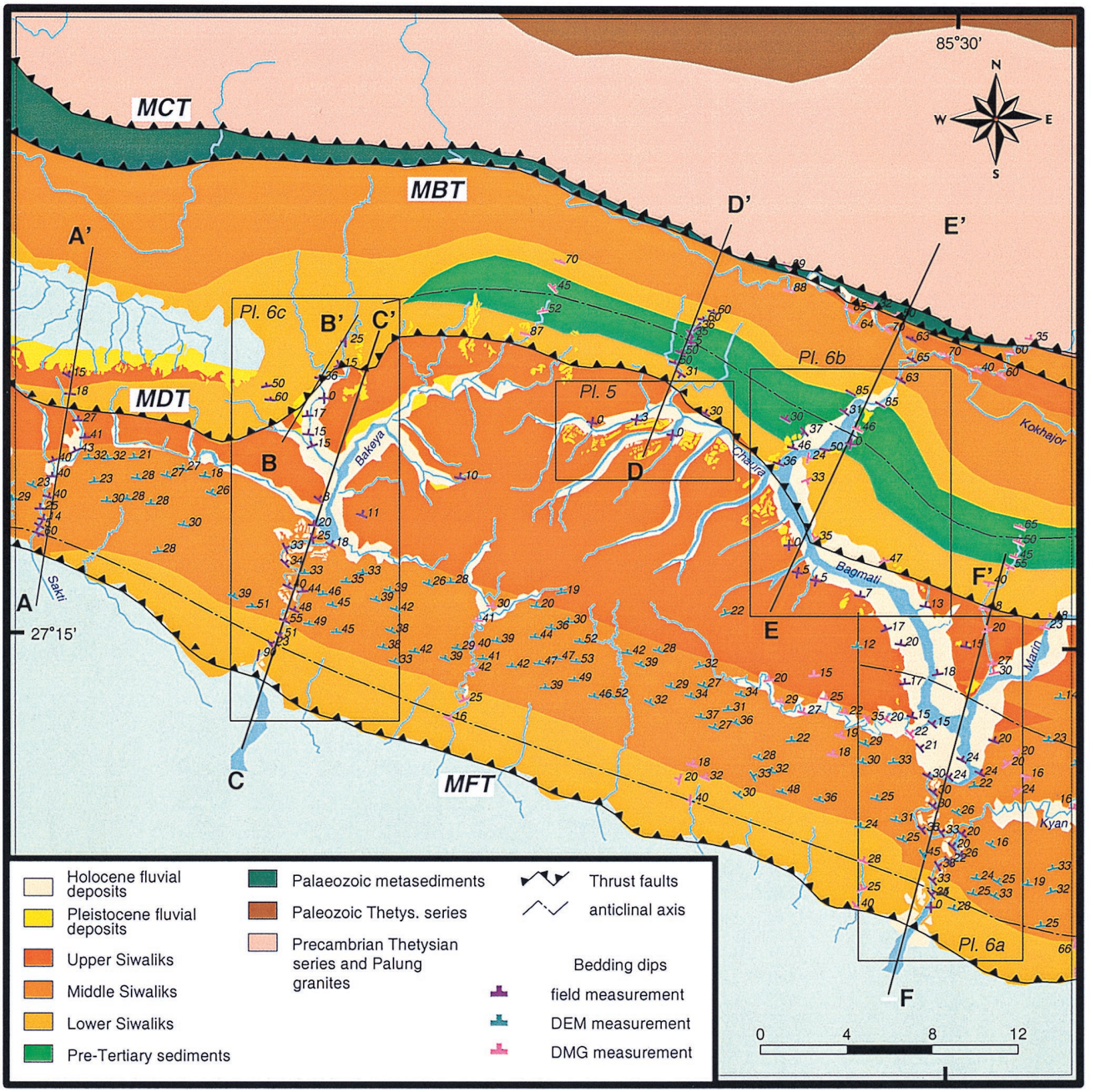

Plate 1. Geology of the study area (see box in Figure 1 for location). The map was drawn on basis of traverses along the Bagmati, Bakeya, Sakti, and Devjhar Rivers (Plate 2), and on a Landsat thematic mapper (TM) image (Plate 3) and a digital elevation model (DEM). We also benefited from a draft of a map in preparation (courtesy of DMG). Dips were measured in the field or from the DEM. Note the characteristic monoclinal geometry of the southern belt along the MFT. The different boxes correspond, from the right to left, to Plates 6c, 5c, 6b, and 6a.

2.2. Stratigraphic and Structural Description of the Study Area in the Siwalik Hills

The molasse deposits that crop out in the sub-Himalayan hills all along the Himalayan arc consist of claystones, siltstones, sandstones, and conglomerates of upper Miocene to Pleistocene age [*Auden*, 1935]. Palaeontological and magnetostratigraphic studies have long focused on the Siwaliks of Pakistan [*Pilgrim*, 1910, 1913, 1917; *Johnson et al*., 1982, 1979]. More recently, the Siwaliks of central Nepal have also drawn some attention. Sections, along Surai Khola [*Appel et al*., 1991; *Corvinus*, 1988], Tinau Khola [*Gautam and Appel*, 1994], Arung Khola [*Tokuoka et al*., 1986], and Bakeya Khola [*Harrison et al*., 1993] all show approximately the same sedimentary sequence: 3500 to 5500 m thick, deposited between 14 and 1 Ma. Most of this sequence crops out in the study area (Figure 1), where it is characterized by fluvial sediments grading upward into coarser material, dated as younger than 11 Ma [*Harrison et al*., 1993].

The geological map of the sub-Himalaya in the study area (Plate 1) was made on the basis of geological sections along the Sakti, Bakeya, Devjhar, and Bagmati Khola (Plate 2). These

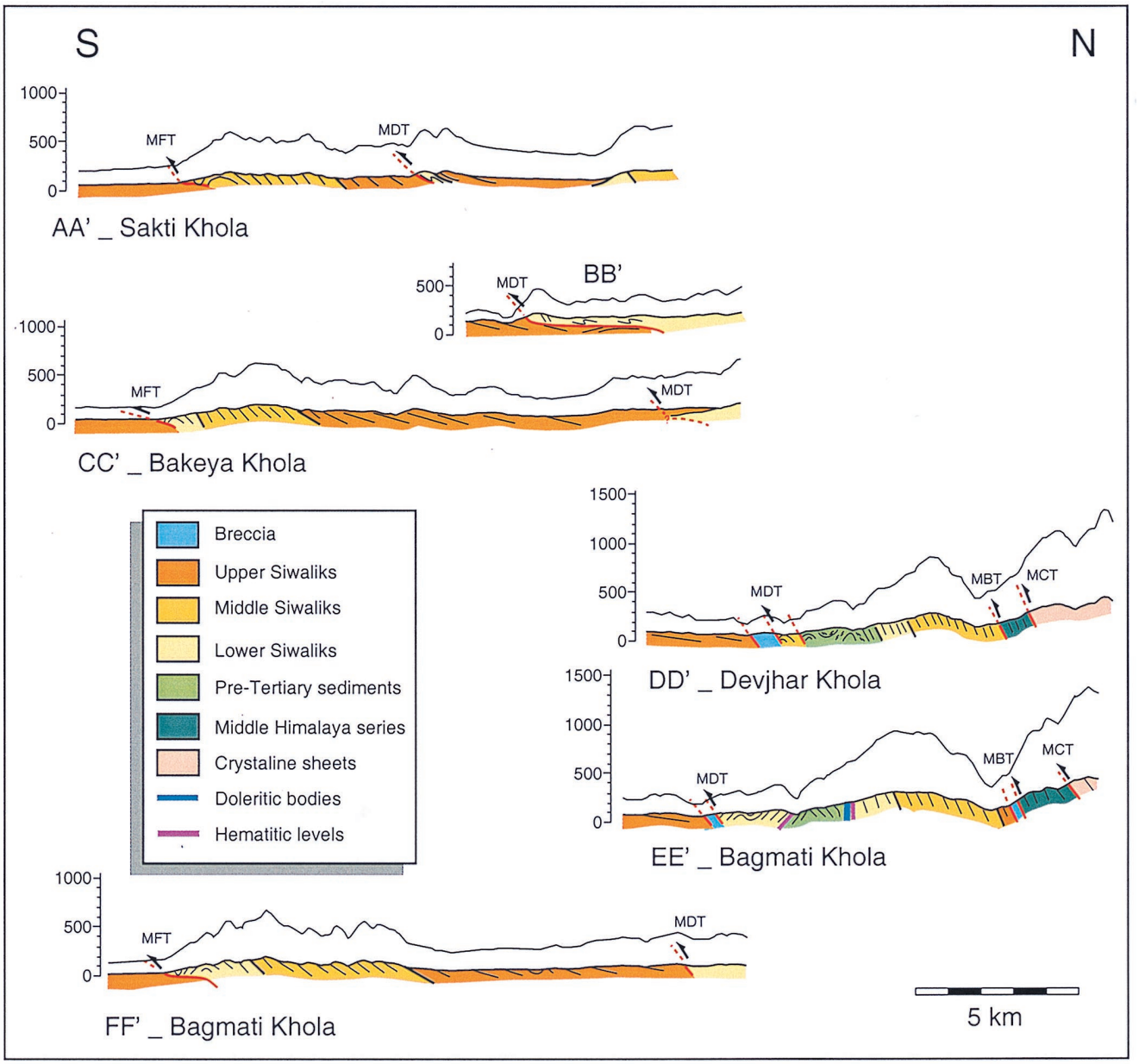

Plate 2. Geological sections along Bagmati, Bakeya, Sakti, and Devjhar Rivers (see Plate 1 for locations). Topography along the sections was extracted from the DEM and is shown with a threefold vertical exaggeration.

sections were extrapolated laterally using the Landsat image of Plate 3 and the digital elevation model (DEM). As may be seen from Plates 2 and 3, the various terrains in the Siwalik Hills have contrasting chromatic and morphologic signatures. The DEM and SPOT images were also used to measure bedding dips. This was possible at many places where clear strata can be traced over several hundreds or thousands of meters across the rugged topography of the Siwalik Hills. South of the MFT, at the southern edge of the Siwalik Hills, the Teraï is an area of active fluvial aggradation where braided and meandering channels flow on a very smooth and flat topography (Plate 3). The Siwalik Hills in the study area are divided in two fold belts. The southern one is the topographic expression of the Main Frontal Thrust fault that is inferred to reach the surface along the southern limb of the fold belt [*Nakata*, 1989]. The other fold belt, ~15 km north of the MFT fold belt, is associated with the Main Dun Thrust (MDT). Elsewhere in Nepal, the Siwalik Hills are more complex, with several fault zones between the MFT and MBT assumed to merge with a single décollement at depth [*Delcaillau*, 1992; *Mugnier et al*., 1992; *Mascle and Hérail*, 1982; *Hérail and Mascle*, 1980].

The MDT fold belt constitutes a steep monocline with dips around 65° to the NNW (Plates 1 and 2). This belt involves ~500 m of pre-Tertiary sediments, mainly reddish-maroon quartzites and gray shales in the lower part. Some doleritic intrusions are found in the topmost quartzites [see also *Gautam et al*., 1995]. The presence of pre-Tertiary rocks is not a common feature of the Siwalik fold belt but also has been reported ~50 km east of our study area, north of the Kamla Khola [*Mascle and Hérail*, 1982]. The incompetent shales show

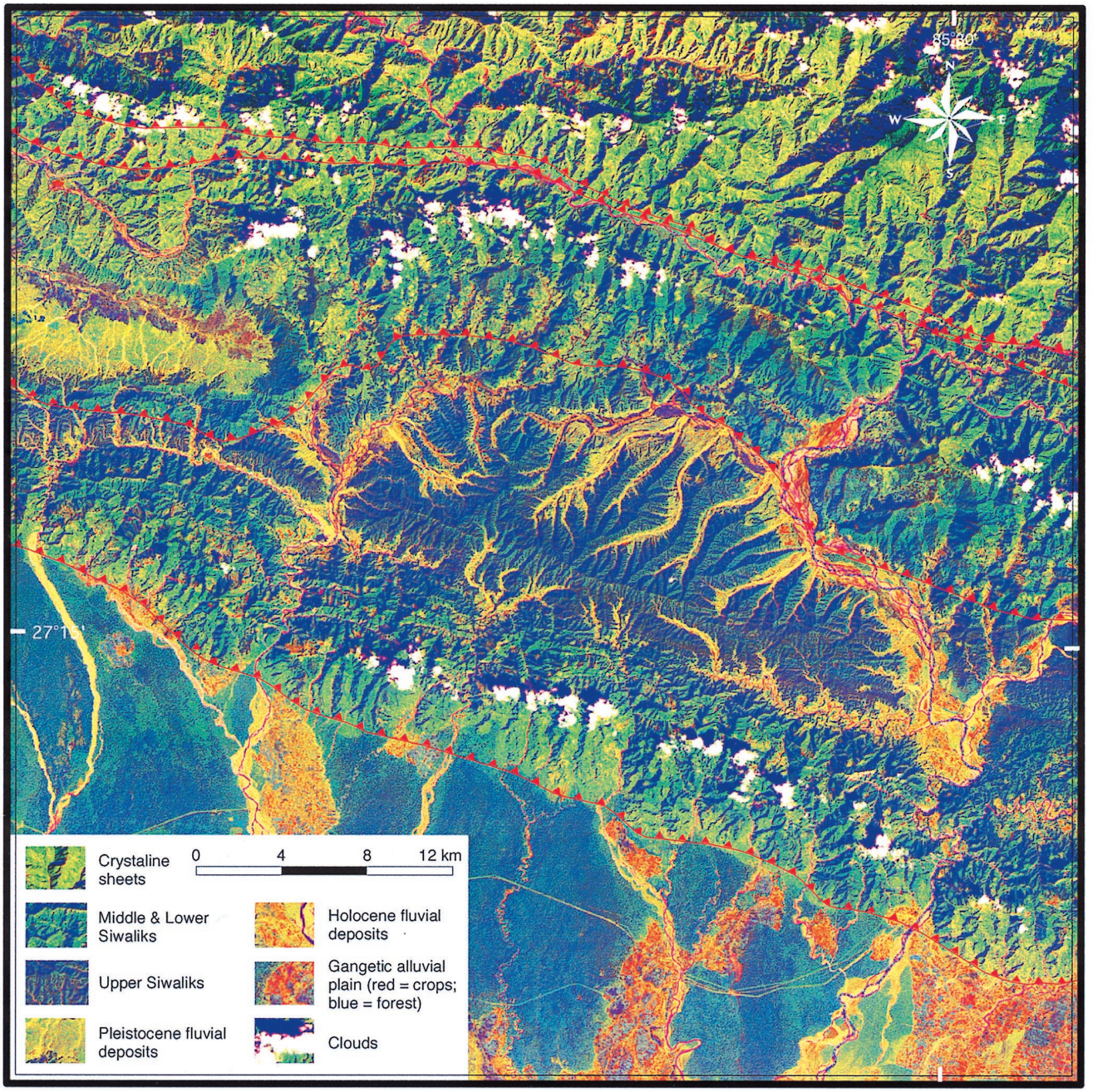

Plate 3. The Landsat TM image of the study area (linear combination of channels 1, 2, 3, 4, 5, and 7) displays contrasting spectral response for the different geologic units. The conglomeratic units appear in dark blue-green colors; the crystalline units, north of the MBT, appear in light green, and the Middle and Lower Siwaliks sandstone units show intermediate colors. The cultivated, Holocene terraces appear clearly in red colors.

meter-scale folds. Small-scale folds and strongly fractured rocks are also found in the Lower Siwaliks at the southern edge of the MDT belt. A 10- to 100-m-thick breccia zone defines the MDT at base of this deformed frontal wedge (Plate 2). It contains essentially angular to subangular sandstone blocks with sparse pre-Siwaliks material.

The MFT fold belt makes a gently inclined monocline with constant strike at on average N105°–110° and dips increasing almost regularly from 0 to 10° on the back limb to 30°–50° (Plates 1 and 2). The steepest values, just north of the MFT, are found primarily in the western part of our study area, around the Bakeya River. Along this reach of the Bakeya the sandstones are continuously exposed and do not display an important internal deformation but do show rare meter-scale fractures. By contrast, at the front of the hills the Lower Siwalik claystones and siltstones are affected by numerous meter- to decameter-scale faults and folds, which define a deformed frontal wedge.

2.3. Depth to the Basement and Balanced Cross Sections

The sections in Plate 2 can be balanced by interpreting both folds associated with the MFT and MDT as fault bend folds [*Suppe*, 1983] associated with curved ramps that root into the same décollement (Plate 4). Although pre-Tertiary units crop

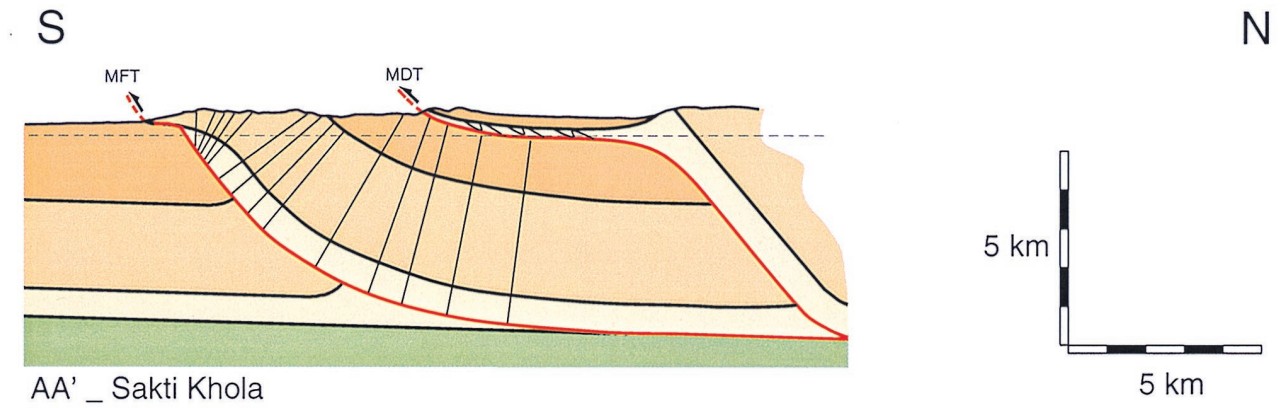

AA' _ Sakti Khola

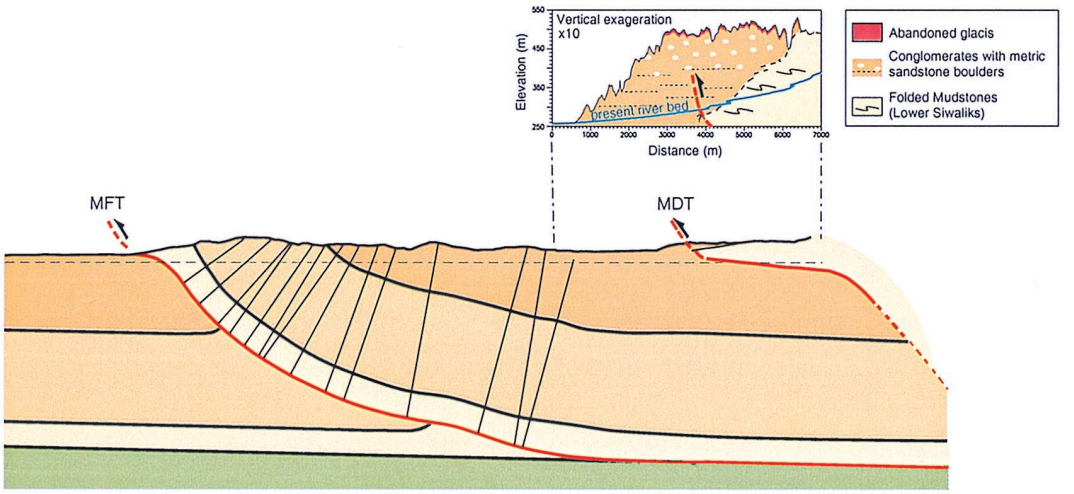

CC' _ Bakeya Khola

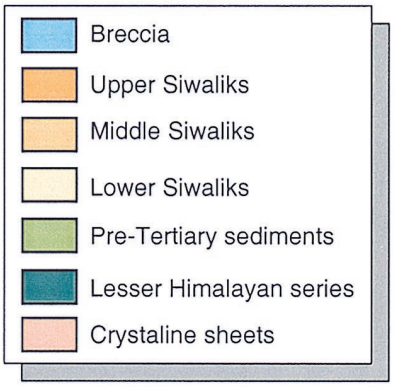

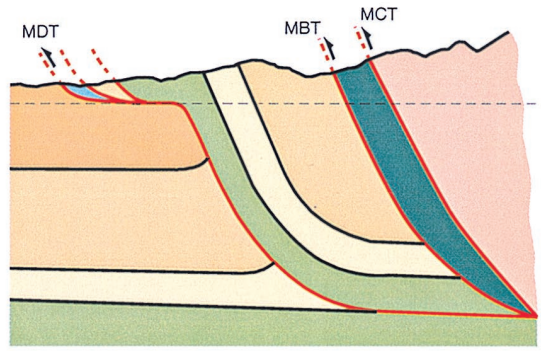

DD' _ Devjhar Khola

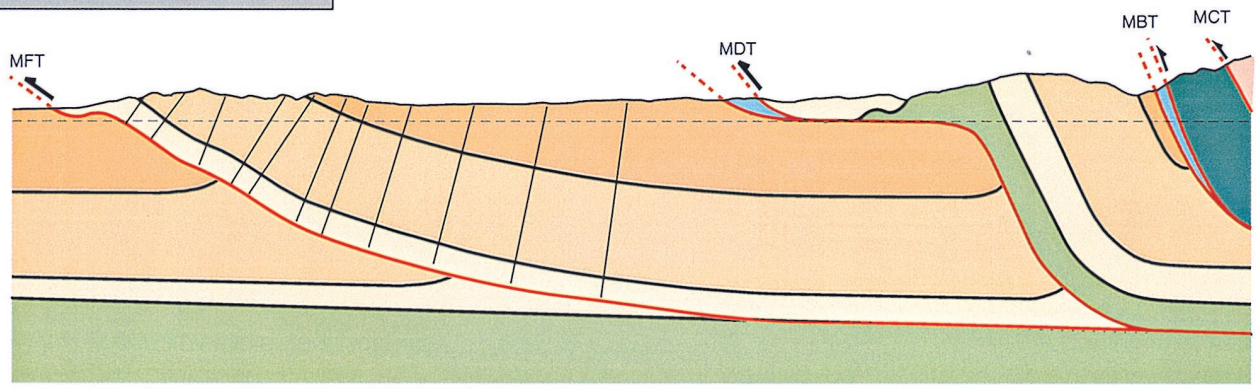

FF' + EE' _ Bagmati Khola

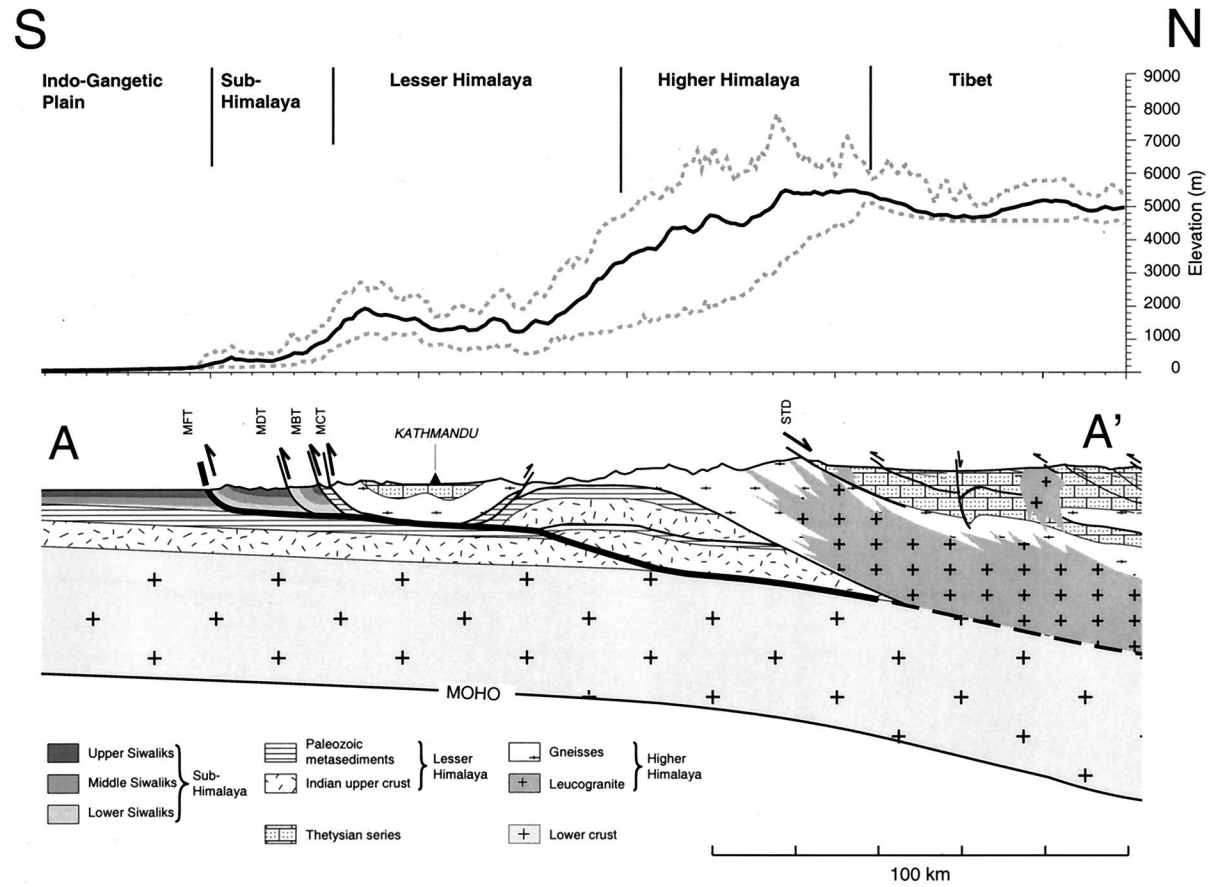

Figure 2. Geological cross section across the central Himalaya of Nepal (see Figure 1 for location) modified from *Brunel* [1986], *Schelling* [1992], and *Pandey et al*. [1995]. The thick dashed line that follows the MCT beneath the Higher Himalaya and southern Tibet roughly coincides with the midcrustal reflector seen 200 km east by the INDEPTH profile [*Zhao et al*., 1993]. The mean (solid line), maximum and minimum elevation profiles (thick dashed lines) within a 50-km swath along the section are also shown (top).

out locally in the MDT fold belt, our observation across the MFT folds and observations in adjacent areas of the Nepalese sub-Himalaya suggest that the décollement lies at the contact between the Lower Siwaliks and the pre-Tertiary basement. The balanced sections imply depths to the basement of 4700–5000 m, comparable with the estimates of *Schelling* [1992a] along the Bagmati (5500 m) and *Harrison et al*. [1993] along the Bakeya (4500 m). For comparison, *Appel et al*. [1991] obtained a depth to the basement of 5500 m along the Surai Khola.

Petroleum exploration data in the Teraï also provide some constraints on the depth to basement and the geometry of the Siwaliks deposits. A well at Raxaul (Figure 1), 40 km to the south of the MFT at Kermaya reached the bottom of the Siwaliks at a depth of 4100 m [*Sastri et al*., 1971]. Below, the drill well penetrated reddish-maroon Vindhyan quartzite units and cut two levels of volcanic rocks, similar to the doleritic bodies that we have shown in the northern belt along the Bagmati. In addition, numerous seismic lines have been acquired in the Teraï [*Department of Mines and Geology* (*DMG*), 1990]. The seismic profile from Kermaya to the Indian border, near Raxaul (line 53, Figure 1), can be used to extrapolate the basement geometry. It shows four clear seismic reflectors dipping gently to the north with gentler slope at shallower depths. These data suggest a north dip of the basement of ~2.5% (Figure 3), consistent with the expected flexural bending computed from a simple thin shell elastic model [*Lyon-Caen and Molnar*, 1985] (Figure 3). When the depth of the basement found at Raxaul is extrapolated northward according to this estimated dip, it appears to connect approximately with the décollement obtained from the balanced cross sections (Figure 3). We will see that fault bend fold geometry provides a simple method for describing the instantaneous kinematics at the surface.

Plate 4. (opposite) Balanced sections corresponding to the sections shown in Plate 2. Sections EE′ and FF′ along the Bagmati River were merged to form a single continuous section. They have been balanced by interpreting both folds associated with the MFT and MDT as fault bend folds associated with curved ramps that root into the same décollement. The Bagmati and Bakeya sections (FF′ and CC′) provide consistent rooting depth, around 5 km deep. North of the Bakeya section, the inset shows an undeformed old surface tapping the frontal deformed wedge of the MDT (topography is shown with a tenfold vertical exaggeration).

3. Description of the Terraces Along Bagmati and Bakeya Rivers

3.1. Fluvial Terraces and Drainage Pattern

Fluvial terraces along the rivers crossing the Siwalik Hills have long been interpreted as a record of active tectonics

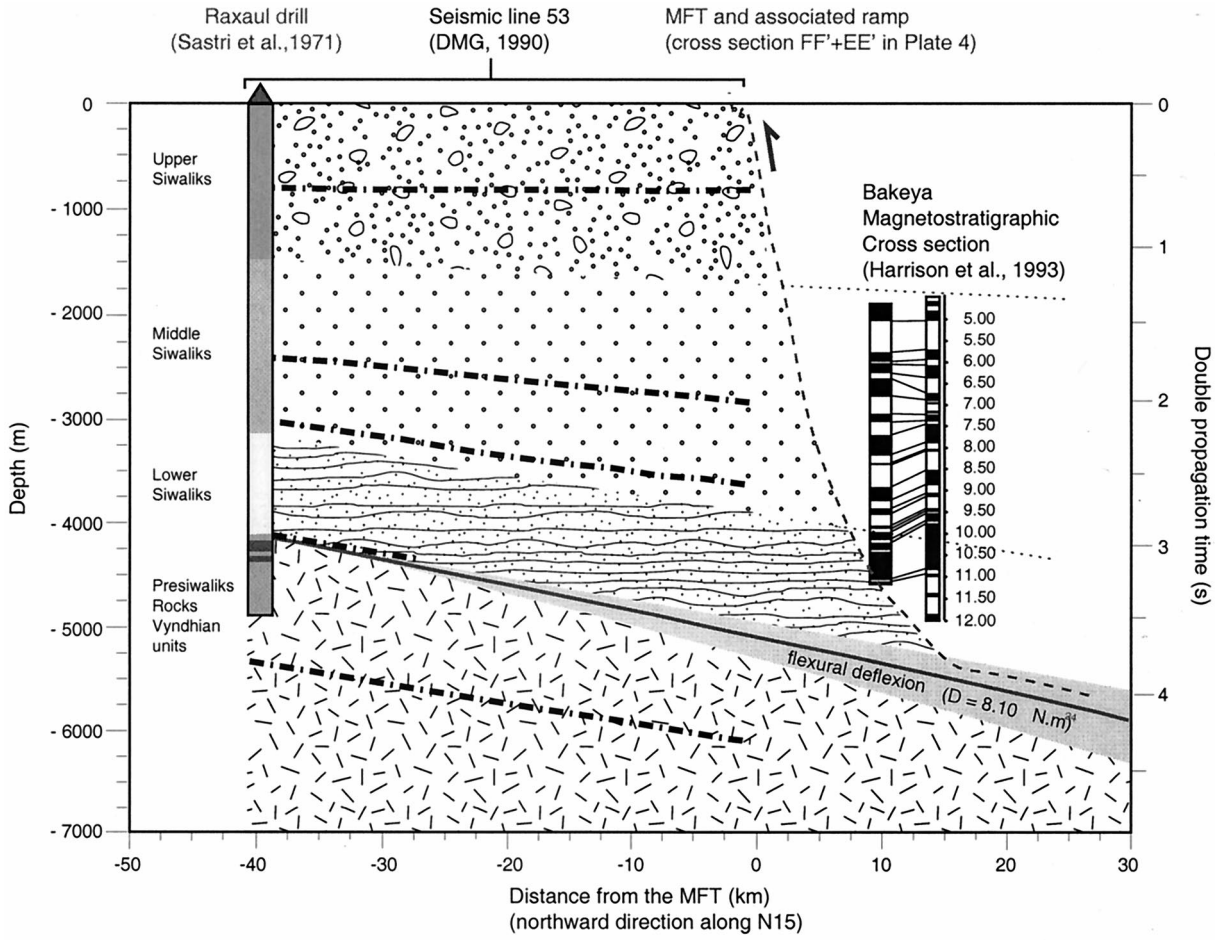

Figure 3. Sketch showing the various constraints on the geometry of the Indian pre-Tertiary basement from the Raxaul drill hole to the MFT. The depth to the reflectors visible on seismic line 53 (thick dash-dotted lines) was calibrated assuming that the deep reflector at 3 s two-way travel time on line 52, which runs near Raxaul, corresponds to the 4100-m-deep basement observed in the drill hole (average velocity of 2.85 km/s). These dip angles are in agreement with the basement dip angle computed from flexural loading of a broken thin elastic plate. In keeping with the results of *Lyon-Caen and Molnar* [1983, 1985] and their computed boundary conditions on the northern edge ($x_0 = 125$ km, $x_0' = 200$ km, applied moment, $M_0 = 4.0 \times 10^{17}$ N, and force $F_0 = 3.0 \times 10^{12}$ N/m), we varied the plate rigidity between $D = 1.$ and 0.4×10^{25} N m (lightly shaded area). We used $\rho = 2.7 \times 10^3$ kg/m^3 for the range topography and $\rho = 2.2 \times 10^3$ kg/m^3 for the sediment filling. The extrapolation of the basement from Raxaul to beneath the MFT is consistent with the depth of the détachment inferred from the balanced sections along the Bagmati (thin dashed line) and Bakeya. The magnetostratigraphic scale along the Bakeya section [*Harrison et al.*, 1993] is shown according to palinspastic restoration of the section. See Figure 1 for location of Raxaul drill hole and seismic lines 52 and 53.

[*Iwata et al.*, 1984; *Iwata and Nakata*, 1986; *Delcaillau*, 1992; *Kimura*, 1995]. In the study area, between the MFT and MBT, we have documented further evidence of deformation from terraces along the two main rivers crossing the MFT fold belt, the Bagmati and the Bakeya Rivers.

Upstream of the Siwalik Hills, the Bagmati River drains an area of about 2500 km^2 that extends across the Lesser Himalaya. The river has cut deep, narrow gorges where it flows across the sandstones units of the MFT fold belt (Plates 1 and 3). Farther north, on the back limb of the MFT fold, the river flows into the unconsolidated Upper Siwaliks and Quaternary conglomerates of the Chaura-Marin Dun. There, despite long-term reincision into this former piggy-back basin, a 500-m-wide braided channel extends north from the confluence with the Marin River up to the anticlinal axis of the MDT fold (Plate 1). This may indicate a recent, moderate filling episode of the Bagmati River in the Chaura-Marin Dun. Notwithstanding variations in channel and valley width, the Bagmati River is characterized by a nearly uniform gradient of 0.27% over a 40-km-long reach from 10 km south of the MFT up to the MDT anticlinal axis (Figure ED1[1]). Upstream, the channel slope steepens to 0.7%. Owing to its large drainage area, the Bagmati River has apparently maintained a dynamic equilibrium in spite of the probable tectonic perturbation in the frontal Siwalik Hills.

[1]Supporting Figures ED1–ED5 are available on diskette or via Anonymous FTP from kosmos.agu.org, directory APEND (Username = anonymous, Password = guest). Diskette may be ordered from American Geophysical Union, 2000 Florida Avenue, N.W., Washington, DC 20009 or by phone at 800-966-2481; $15.00. Payment must accompany order.

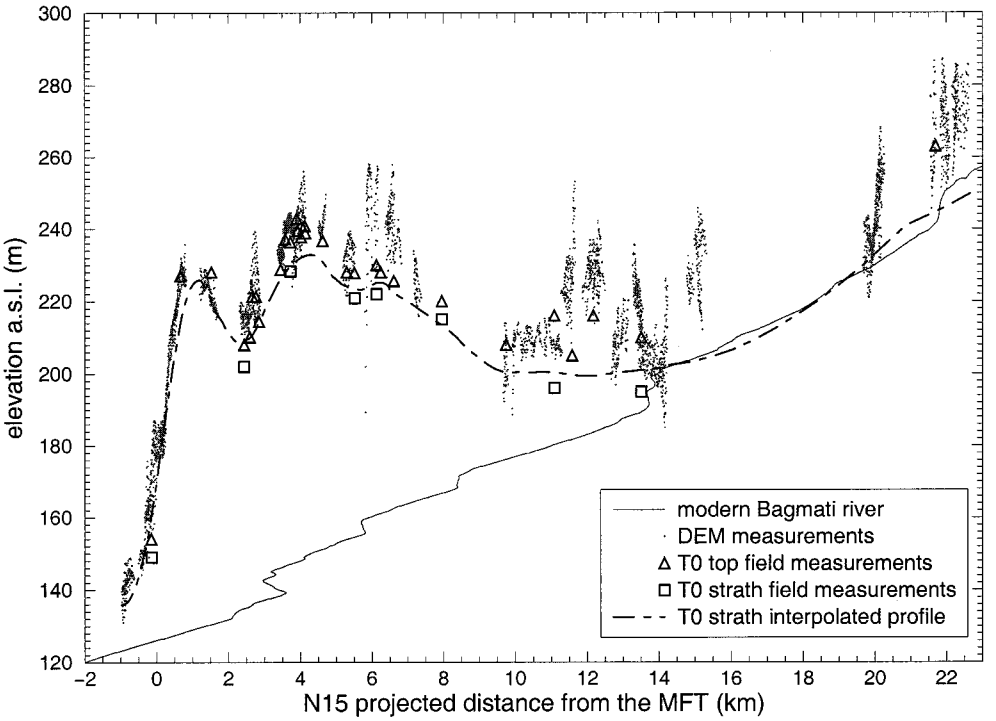

Figure 4. Comparison of field and DEM measurements of elevation of T_0 along the Bagmati River. Elevations of the strath level (squares) and at top of the gravely and silty cover (triangles) are shown. The DEM measurements (dots) should be comparable to the field measurements of the top of the terrace. The dashed line is the mean elevation profile of the strath level computed according to procedure described in Appendix A. Above the MFT ramp tip ($x = 0.5$ km), the southward tilting of the profile is constrained by a wide, continuous, single terrace (the 1-km north-south elongated T_0 terrace on Plate 6a). There, two field measurements, at the extremities of this terrace, and numerous DEM measurements constrain the profile.

The Bakeya River has a watershed 8 times smaller than that of the Bagmati and drains principally the two Siwaliks fold belts. Where the river cuts across the MFT fold, it narrows and shows a 2- to 3-km-long knickpoint that interrupts the 0.43% regional slope (Figure ED2). This knickpoint is not related to any clear structural or lithological contrast and is thus inferred to be of tectonic origin. It suggests that the Bakeya River is not able to maintain a uniform gradient in the zone of active uplift, probably due to a lower stream power than the Bagmati.

3.2. Terrace Mapping and Field Survey: Methodology

The terraces in the study area were mapped from air photos and SPOT images. They were classified according to their spectral signature on the Landsat image (Plate 3). The terrace classification was calibrated and improved in the field by looking at the weathering color, facies, and thickness of the alluvial veneer and of the overbank deposits. Correlation of disconnected treads was based on the characteristics of the overlying material and where possible on the relative altitudes from reach to reach (Plates 5 and 6). The youngest terraces are characterized by a low degree of weathering (color of the silt and sand from beige to orange), while the older levels are more intensely and deeply weathered (silt and sand from deep orange to red). In keeping with a common usage for the area [e.g., *Iwata and Nakata*, 1986; *Delcaillau*, 1992] we will refer to the former as Holocene terraces and to the latter as Pleistocene terraces. A more precise chronology will be discussed in section 3.6.

Elevations were measured on the digital elevation model or in the field. The DEM is a 20 × 20 m grid of elevations with a 1 σ uncertainty on elevations of 15 m. This uncertainty reflects the accuracy of the registration of the two stereographic SPOT images. Other sources of errors are possible, including dissection of the terraces by gullies, colluvium accumulation, and trees. In the field, terrace elevations were measured using digital altimeters with an accuracy of 3–4 m after correction for barometric changes. Where possible, we measured the elevation of the top of the fill material and gravels and of the strath level. The field measurements of the top of the fill compare well with the DEM measurements on average, but there is a greater scatter in the DEM measurements (Figure 4). In order to construct strath level profiles (see procedure in Appendix A), in particular across the MFT fold, elevations measured at the top of the fill were corrected for the thickness of the overlying cover. To do so, the thickness of the fill was interpolated linearly between the measured points in the field (Figure 4).

3.3. Pleistocene Terraces and Tectonic Activity of the MDT

Pleistocene terraces are preserved on the back limb of the frontal fold and south of the anticlinal axis of the MDT fold belt and have been generated by the main rivers and their tributaries. Some present a clear strath level, but most of them possess a thick (>10 m) alluvium and colluvium cover. Erosion by diffusion processes and dissection or the deposition of colluvium significantly affects the overlying material and soil profiles and prevents extensive terrace correlation. However, these terraces may still help to qualitatively characterize the tectonic activity around the MDT.

For example, a flight of seven inset terraces, mostly Pleistocene, is present along the Chaura River, a Bagmati tributary, where it flows along the northern limb of the MFT fold (Plate 5; see Plate 1 for location). These terraces are unpaired and systematically lie on the southern side of the valley. These terraces indicate that the Chaura River has migrated northward during incision and is presently cutting the front of the MDT fold belt. This pattern is actually consistent with northward tilt of the back limb of the MFT fold.

Along the Bagmati River, the terraces, for which we have inferred Pleistocene ages, were divided into three families. Pl_1 terraces present a highly weathered soil profile >5 m thick; Pl_2 terraces are characterized by a 3- to 5-m-thick red horizon; and Pl_3 are characterized by a deep orange to red, 1- to 3-m-thick, weathered horizon. These three groups of terraces seem to have been tilted northward on the back limb of the MFT fold, with an increasing degree of back tilting from Pl_3 to Pl_1. Some of them extend north of the MDT (Plates 1 and 6b). Despite a poor reliability on terraces correlation, the fact that the patches form a continuous trend at a nearly constant elevation suggests no vertical offset at crossing the MDT or at most 20 m given the uncertainty on elevation measurements (Plate 7a). Similarly, in the northern Bakeya valley, an abandoned surface, older than Pl_1 terraces and 250 m above the present river, is tapping the Lower Siwaliks of the frontal deformed wedge associated to the MDT fold (inset in Plate 4). This old surface, characterized by a 10-m-thick weathered soil profile, has not been significantly deformed. It suggests that few internal deformations of the frontal wedge, and probably a limited slip on MDT, have occurred since surface reincision.

In both valleys the Pleistocene terraces indicate a clear incision, probably related to the northward tilt of the back limb of the MFT. However, they suggest minor differential uplift between the Dun and the northern Siwalik belt and low level tectonic activity on the MDT. Only a few remnants of Pleistocene terraces could be found across the MFT belt, where they have probably been eroded away. By contrast, abundant remnants of Holocene terraces are found in the valleys that cut across the MFT fold belt along the Bagmati and Bakeya Rivers (Plates 1 and 6). In sections 3.4–3.6 we focus on these Holocene terraces to assess MFT activity.

3.4. Description of the Holocene Terraces Along the Bagmati River

Along the Bagmati River, between the MFT and MBT, several levels of Holocene strath terraces may be observed. They lie a few meters above the active floodplain, immediately south of the MFT (Plate 8a) and north of the MFT fold, while they can reach up to 90 m above the present river (apr) in the core of the belt (Plate 8b). This geometry suggests that the terraces have been warped after they were generated.

Along the narrow section of the Bagmati River, from the MFT up to the confluence with the Marin River, the terrace remnants can be followed nearly continuously from reach to reach (Plate 6a). There we recognized four different terrace levels. The most prominent terrace level, T_0, forms well-preserved flat treads, 100–300 m wide. The strath is capped by a 3- to 4-m-thick gravel, overlain by 2–3 m of fine, beige to orange sand and silts (Figure 5). In the core of the monocline, T_0 remnants lie 70–95 m apr. The second most prominent level, T_3, is the lowest preserved level. The strath is generally well exposed and appears to be covered by a thicker veneer than that associated with T_0. It consists of 2–4 m of boulders and gravel overlain by 5–8 m of light beige sands and silts (Figure 5). Along the canyon, these remnants are not as wide (30–100 m) as the T_0 remnants. By contrast, particularly wide and well-preserved remnants are observed at the entrance of the canyon. Although they are generally poorly exposed, two terrace levels, T_1 and T_2 (Plate 6a), were recognized, and their remnants were correlated according to their elevations between those of T_0 and T_3.

Within a few kilometers north of the canyon, the T_3 terrace merges with the floodplain and the veneer capping the strath may thicken upstream and form a possible fill terrace below the floodplain up to the MDT anticlinal axis. The other Holocene terraces lie only 0 to 30 m apr (Plates 6a and 6b) so that the lowest cannot be easily distinguished from the present Bagmati floodplain. Moreover, the Upper Siwalik conglomerates, formed of poorly consolidated material very similar to the terrace gravels, are eroded by numerous gullies. These gullies deposit alluvial fans on the Bagmati floodplain, which may obscure the terrace record. Between the MBT and MDT the Holocene terraces seem to lie between 5 and 10 m apr. We did not observe any straths in that area and inferred a relatively thick veneer.

In Plate 7a, the elevations of all the terrace remnants along the Bagmati River are projected onto a plane striking perpendicular to the fold axis. Along the narrow section of the river, T_3 forms a continuous profile that mimics the T_0 profile, with a lower degree of back tilting along the back limb of the fold. Although T_1 profile is less constrained and its southern section incomplete, T_1 profile seems to follow a similar pattern (Plate 7a). The ensemble of Holocene terrace levels thus indicates persistent active folding at the MFT.

3.5. Description of the Holocene Terraces Along the Bakeya River

Although less abundant than along the Bagmati, fluvial terraces are also found along the Bakeya River, in particular in the northern section of the gorge (Plate 6c). The most prominent and highest level is similar to T_0 along the Bagmati River. It is characterized by a strath level covered by 3–4 m of boulders and gravels overlain by 1.5–2.5 m of light beige to orange sands and silts. A particularly large remnant of T_0, 200 m wide, lies in the core of the fold, ~130 m above the present river channel (Plates 6c and 7b). This level is also well preserved at the entrance of the narrows where reaches can be found on both sides of the river (Plates 6c and 7b). As along the Bagmati River, the other prominent terrace is the lowest preserved level. The lowest strath lies 10–30 m above the present river channel. It is covered with 2–5 m of boulders and gravels, overlain by 2–4 m of light beige sands and silts. Owing to the similarities with the terraces along the Bagmati River, these two levels will be referred to as T_0 and T_3, respectively. Between T_0 and T_3, other terrace remnants appear to define two intermediate levels and could correspond to T_1 and T_2 (Plate 7b).

North of the canyon, preserved terrace remnants are sparse and any correlation would be speculative. As along the Bagmati River, the Bakeya terraces have recorded active folding at the MFT, with a maximum amplitude along the southern part of the canyon (Plate 7b).

3.6. Chronology of the Holocene Terraces

Fragments of charcoal have been sampled on the fluvial terraces along both valleys (see location of samples in Plates 6,

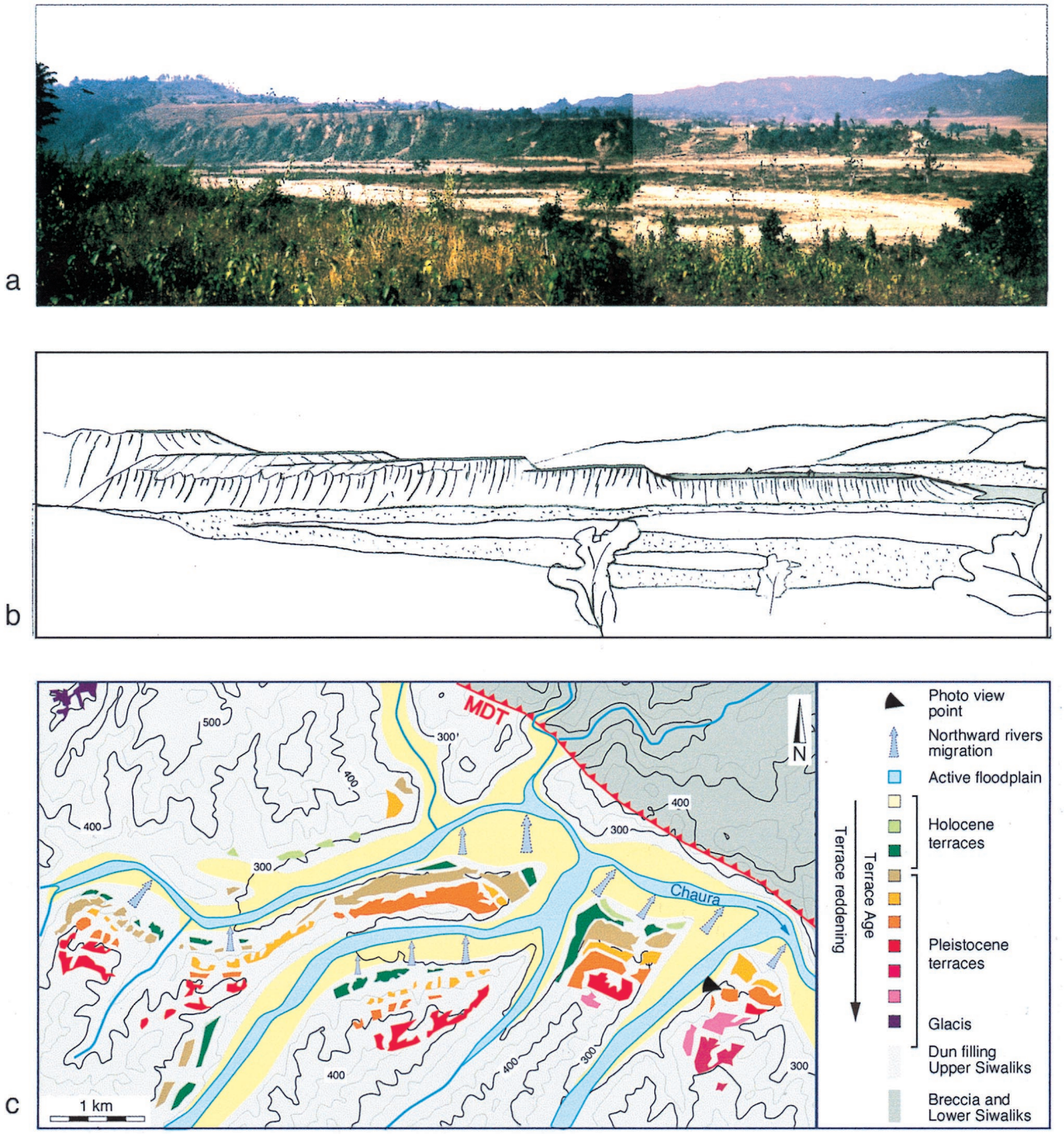

Plate 5. (a) and (b) View toward the west and (c) geomorphological map of seven inset terraces along the Chaura Dun (see the box in Plate 1 for location). These terraces suggest northward migration during incision of the Chaura River. This migration probably resulted from the northward tilt of the northern limb of the MFT fold during fold growth and from the greater sediment supply in provenance from the southern drainage.

7a, and 7b). Carbon 14 ages were obtained on 19 samples and were calibrated according to the dendrochronological scales of *Stuiver and Becker* [1993] and *Pearson et al*. [1993] (Table 1). They all yield Holocene ages (Table 1) younger than 10 calibrated (cal) ka. Surprisingly young ages were obtained from some samples collected in the silty cover of some terraces (Table 1).

In order to evaluate our age control we dated several samples from a single site on T_0 approximately halfway down the Bagmati canyon (site Ba1 identifiable by symbol SIW54 in Plate 6a). All samples were collected from an outcrop at the head of a fresh gully lying about 200 m away from the valley flanks (Figure 9a). There the terrace top lies 90–95 m apr (Plate 7a). The samples were taken at different elevations relative to the strath and top of the fill (Figure 5a). Sample SIW-54, obtained from a sandy lens within the fluvial gravel, was dated at 9.0–9.2 cal ka. Since the sandy lens is overlain by 1 m of pebbly to bouldery gravel, we assume it was deposited on the active channel floor. Between the sandy lens and the strath, the 3.5-m-thick gravel indicates that the strath aban-

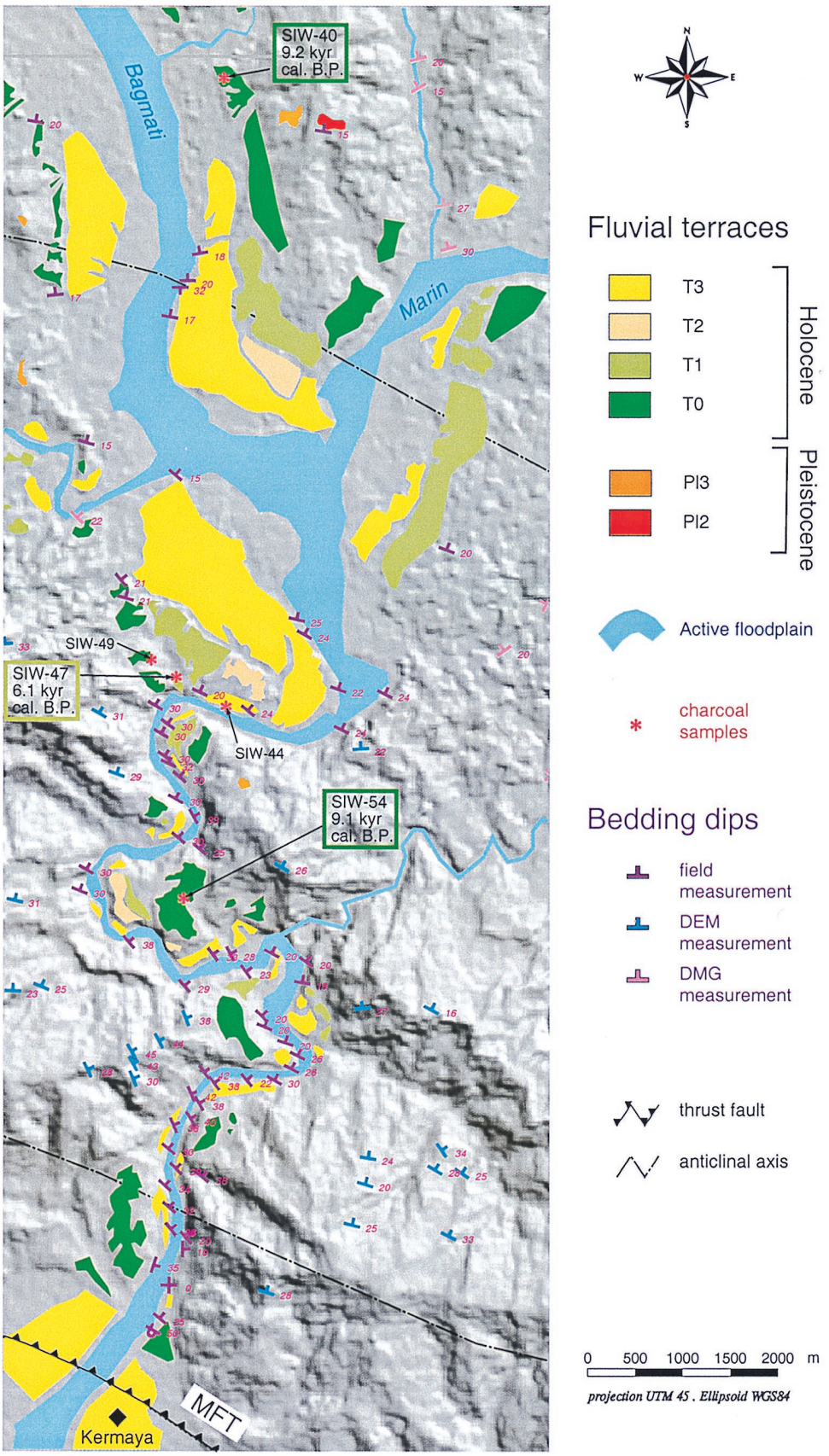

Plate 6a. Map of the terraces along the Bagmati River (southern map) where it cuts across the MFT fold. Shaded background is the DEM topography. Bedding dips measurements from the field, *DMG* [1990], or from the DEM are also indicated.

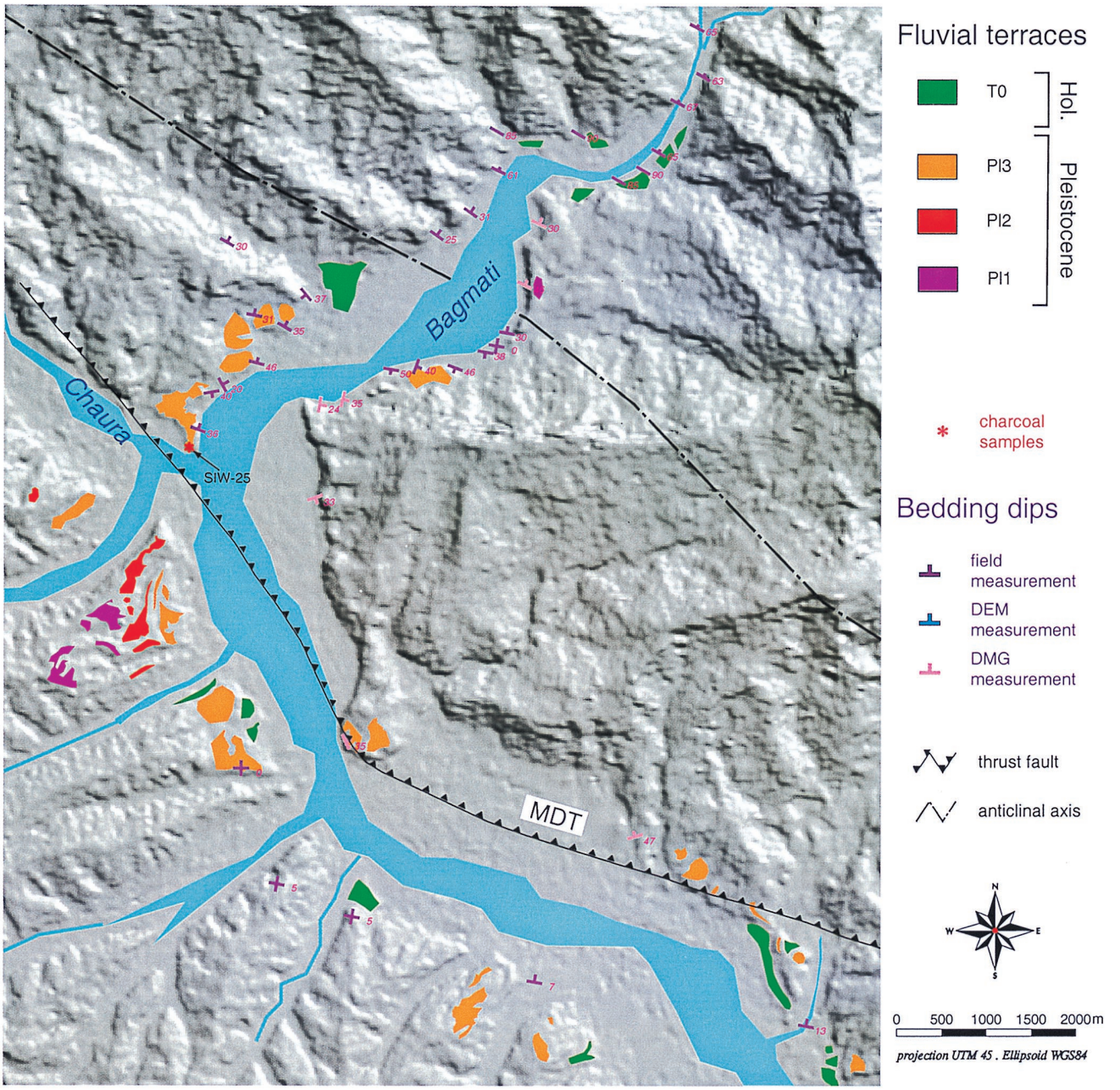

Plate 6b. Same as Plate 6a, except northern map.

donment was followed by an aggradation phase. Given the large volume of sediments carried by the Bagmati, this phase was probably short, of the order of 100 years. This sample may therefore be taken to provide a reliable estimate of the age when strath abrasion stopped. Sample M1 was collected at the bottom of the silty sequence topping the gravels (Figure 5a). It yields an age that postdates SIW-54 by only 200 years (note that error bars are of the order of 100 years, Table 1). These close ages indicate that the gravels probably accumulated rapidly and were soon covered by silts. The three other samples from the silt sequence yield younger ages of 7.2 cal ka, 6.4 cal ka, and 3.3 cal ka, respectively, consistent with their relative stratigraphic positions (Figure 5a and Table 1). We conclude that at this particular site, the river has entrenched 85 m since about 9.1 cal ka, yielding a mean incision rate of 9.2 ± 0.4 mm/yr.

Silty terrace top deposits have commonly been interpreted as overbank deposits, for example, by *Merritts et al*. [1994] or *Personius* [1995]. During major monsoonal floods the water level may rise up to 10 m in the Bagmati narrow. Assuming a constant 9–10 mm/yr incision rate during the Holocene, this would allow for the age of the silty cover to lag by ~1 kyr at most behind the age of abandonment of the strath. The youngest samples, dated between 6.4 and 3.3 cal ka, probably do not fit such a scenario. More likely, they have been progressively buried, either through bioturbation or agricultural activity or by colluvium sourced from the valley side. In considering this terrace section it is our view that the age of abandonment of a

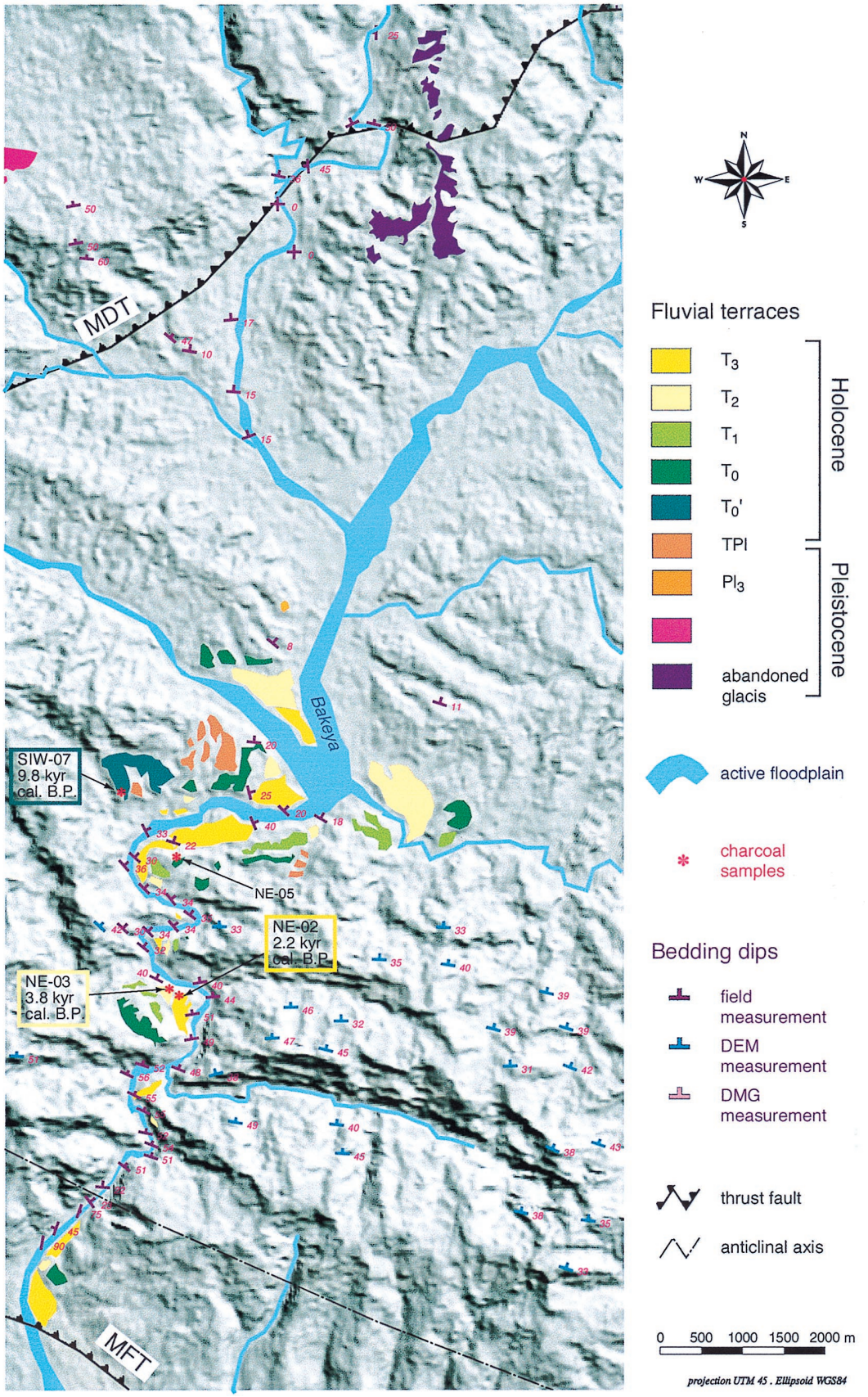

Plate 6c. Same as Plate 6a, except for the Bakeya River.

strath terrace and its cover of bedload deposits may reasonably be estimated by charcoal sampled at the bottom or below the silt cover, rather than by samples collected within the silt cover.

The age of T_0 along the Bagmati River could also be constrained at another site, 10 km farther upstream (SIW-40, Plate 6a). There, several alluvial/colluvial fans merge with T_0. In one of them, a sample was found at the base of the silty sequence covering the gravels. Its age of 9.2 cal ka ±200 cal years ago (Table 1) suggests that the Bagmati T_0 strath and the adjacent lateral fans were abandoned synchronously at the two sites. One simple hypothesis would be that terrace remnants were abandoned synchronously all along the Bagmati canyon. Although sediment wave propagation [*Weldon*, 1986] or knickpoint retreat [*Seidl and Dietrich*, 1992] may promote terrace diachronism, strath terraces, beveled into bedrock, are most likely to represent ancient reaches in equilibrium [*Bull*, 1991; *Merritts et al*., 1994]. Given the relative short length of the studied river section and the age correspondence between SIW-40 and SIW-54, we assume longitudinal synchroneity of abandonment along the T_0 tread.

Along the Bakeya River a sample was collected on the wide T_0' terrace remnant that lies 15 m above T_0 at the northern end of the canyon and corresponds to an abandoned meander. The sample (SIW-07 in Plates 6c and 7b and Table 1) was dated at 9.9 cal ka. Given that this terrace must have been abandoned before T_0, this age is consistent with a proposed age of 9.2 ± 0.15 cal ka for the abandonment of T_0 along both the Bakeya and the Bagmati River (Table 2).

Additionally, the highest terraces, without reddened weathering profiles, were also sampled along the Narayani and Arun River [*Lavé*, 1997], 150 km to the west and 200 km to the east of the Bagmati River, respectively (C1 and C2 on Figure 1). These terraces yielded abandonment ages of 9.0 ± 0.2 and 9.2 ± 0.2 cal ka from ^{14}C dating on charcoals. This suggests lateral synchroneity of abandonment of the early Holocene floodplains along the major rivers crossing the sub-Himalaya. These samples yield very consistent ages, although they were collected at different levels within or slightly above the gravel layer overlying the strath. This confirms that the aggradation phase that followed strath abandonment was short, probably of the order of the error bar on age determination at most.

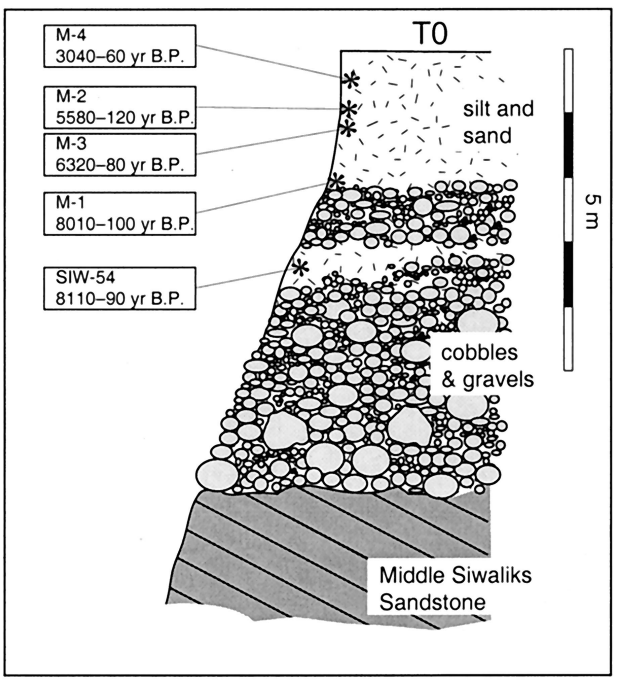

Figure 5a. Schematic section of terrace T_0 at the site along the Bagmati River where samples SIW-54 and M1 to M-4 were collected (Table 1).

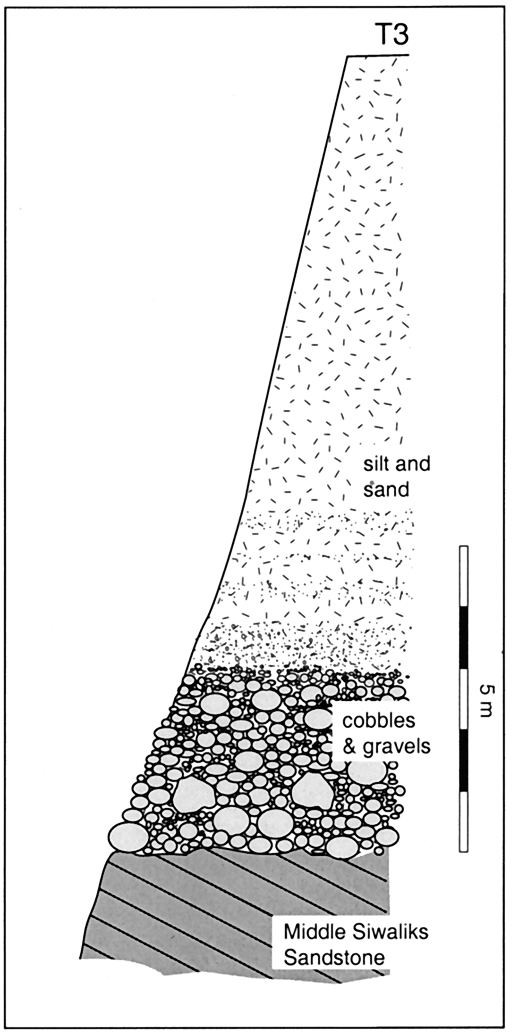

Figure 5b. Schematic section of terrace T_3.

The age of T_1 abandonment along the Bagmati River may be constrained from sample SIW-47 (Plate 6a) at 6.2 cal ka (Table 1). The age of T_2 abandonment is constrained from only one sample, collected along the Bakeya River (NE-3 in Table 1) and dated at 3.7 cal ka. Two samples were collected on T_3, one along the Bakeya River (NE-2 in Plate 6c and Table 1), the other along the Bagmati River (SIW-44 in Plate 6a and Table 1). Sample NE-2 was collected in a sandy lens below some fluvial gravel and can therefore be considered to provide a good estimate of the abandonment of the strath at 2.2 cal ka. The sample SIW-44 was collected at a site where the silt layer lies directly on the strath. A very young age of 0.7 kyr suggests that the 2-m-thick gravel observed elsewhere on T_3 was probably washed out some time after the abandonment of the strath and replaced by late overbank deposits.

Comparison with the results of paleoclimatic studies carried on in south Tibet and India, shows that the four episodes of

Table 1. Description and ^{14}C Dating of Charcoal Samples

Sample	^{14}C Age, ka	Calibrated Age (cal ka)	River	Terrace Level (Sampling Site)	Elevation, m: Beneath the Terrace Top	Elevation, m: Above the Gravels	Stratigraphic Description
NE-2	2200 ± 120	2010–2340	Bakeya	T_3 (Bk1)	−2.5	+1.5	below a gravely level
NE-3	3460 ± 60	3630–3820	Bakeya	T_2 (Bk1)	−1.5	+0.3	in silt
NE-5*	2380 ± 60	2340–2460	Bakeya	T_0	−1.0	+1.0	in silt
SIW-07	9020 ± 170	9720–1090	Bakeya	T_0	−1.6	+0.1	in silt
SIW-44	770 ± 50	660–810	Bagmati	T_3 (Ba2)	−7.0	+0.7	no boulder above the strath
SIW-47	5390 ± 70	6050–6290	Bagmati	T_1 (Ba2)	−3.5	+0.5	in sandy silt
SIW-49*	1630 ± 70	1400–1570	Bagmati	T_0 (Ba2)	−3.0	+0.5	in a sandy silt sequence with very thin gravely layers (possible colluvium origin).
SIW-40	8310 ± 90	9070–9430	Bagmati	T_0	−1.5	+1.5	in sandy silt—strath not visible below 12 m of gravels
M-4*	3040 ± 60	3170–3340	Bagmati	T_0 (Ba1)	−0.8	+1.4	see Figure 13
M-2*	5580 ± 120	6290–6480	Bagmati	T_0 (Ba1)	−1.0	+1.2	see Figure 13
M-3	6320 ± 80	7170–7280	Bagmati	T_0 (Ba1)	−1.2	+1.0	see Figure 13
M-1	8010 ± 100	8650–9000	Bagmati	T_0 (Ba1)	−2.2	+0.0	see Figure 13
SIW-54	8110 ± 90	8960–9190	Bagmati	T_0 (Ba1)	−3.0	−0.8	see Figure 13
SIW-25*	360 ± 60	310–500	Bagmati	Pl_3	−1.5	+0.2	in weathered silts

Sampling sites are reported in Plates 6a, 6b, and 6c.
*Charcoals yielding surprisingly too young ages for terrace abandonment, like SIW-49 into a T_0 remnant 20 m above SIW-47, or M-4 into the same terrace as SIW-54 or M-1.

floodplain abandonment documented in this study are correlated with Holocene climatic transition from wet to dryer conditions [*Lavé*, 1997]. Strath abandonment would be climatically induced and would occur synchronously in the Siwaliks in response to regional decrease in stream power [*Lavé*, 1997]. Despite fluvial response to climate change may be complex and diachronous along the river [*Weldon*, 1986], we believe that for short reaches across the Siwaliks, far downstream of the headwaters, floodplain abandonment is synchronous, as observed for T_0 level. In the following, we therefore consider that the four major terrace levels of Holocene age are isochronous.

Table 2. Characteristics of Modern and Paleochannels of Bagmati and Bakeya Rivers Measured Along the Narrows Across the Active MFT Fold in the Siwaliks

Terrace Level	Proposed Age of Abandonment, cal ka	Width, m	Sinuosity
T_0	9.2 ± 0.15	300–600	1.8
		100–500*	1.25*
T_1	6.15 ± 0.15	170–350	2.0
		100–450*	1.3*
T_2	3.7 ± 0.1	...	...
		>50–70*	...
T_3	2.2 ± 0.2	150–300	2.1
		70–400*	2.5*
Modern river	active	85–170	2.4
		30–150*	1.7*

*Bakeya River.

4. Determination of Holocene Uplift Rates

4.1. Method for Determination of Uplift Rates

The profiles of the various fluvial terraces along the Bagmati and Bakeya Rivers (Plates 7a and 7b) clearly attest to active growth of the MFT fold during the Holocene and Pleistocene, with a progressive northward tilting of the back limb. There terrace ages indicate incision rates as high as 10–15 mm/yr. By contrast, no prominent activity is indicated at the MDT (Plate 7a). South of the Siwalik Hills, a relatively undisturbed pattern of meandering and braided rivers (Plate 3) suggests uniform aggradation. We infer that there must be little, if any, active tectonics south of the MFT.

In order to interpret the observed incision across the MFT fold and to derive the tectonic uplift profile along the two rivers, we need to estimate the geometry of the terraces at the time of their abandonment. If it is assumed that the rivers have maintained constant long profile and horizontal geometry during deformation, the tectonic uplift since abandonment of a floodplain would simply be equal to the incision. We can test this by assuming that the fold has been growing steadily during the Holocene. This approximation makes sense given that the mean recurrence interval of the $M \geq 8$ earthquakes that could activate the fold is at most a few hundred years [*Molnar and Deng*, 1984]. Also Holocene folding represents only an increment of deformation during the 0.5–1 Myr duration of the complete fold history [*Lavé*, 1997]. In that case the incision profiles deduced from two different isochronous terrace treads i and j should be similar with a similarity ratio equal to that of their respective ages. The following equations should apply:

$$I(x, t, t_i) = kI(x, t, t_j) \quad (1)$$

$$k = (t - t_i)/(t - t_j), \quad (2)$$

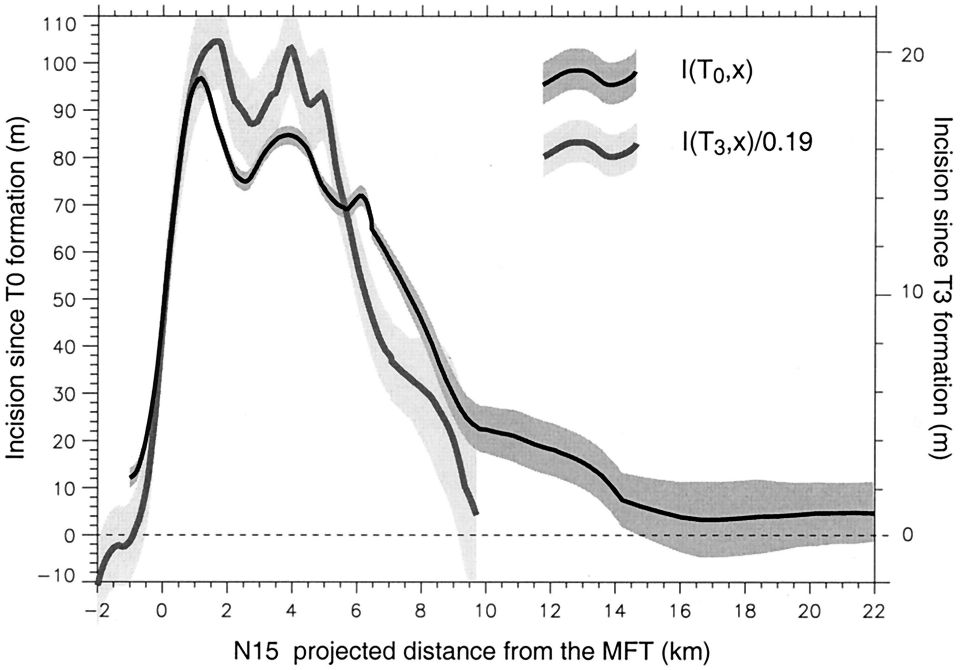

Figure 6. Comparison of incision profiles deduced from T_0 and T_3 along the Bagmati River. Field measurements and DEM measurements constrain the mean profiles (Appendix A). Shaded areas indicate the 1σ confidence interval on the mean profiles computed according to the procedure described in Appendix C. The best homothetic ratio was computed according to a least squares criterion (Appendix D) in order to test the condition given by equation (1). The two profiles are nearly similar, but with some mismatch in particular on the back limb of the fold, where the T_3 surface merges with the present floodplain farther downstream than T_0. This may correspond to a deficit of incision, relative to the average incision rate, since T_3 abandonment. The comparison between the ratio of incision ($I(T_3)/I(T_0) = 0.19$) and the ratio of the age of abandonment of T_3 and T_0 ($(t - t_3)/(t - t_0) = 0.24$) also suggests a deficit of incision.

where $I(x, t, t_i)$ is the incision deduced from the elevation above the present river of the terrace tread T_i at a projected distance x from the MFT along a line trending N15°–20° and abandoned at time t_i before the present time t. Condition (1) is a geometric test that does not depend on the terrace ages or detailed timing of the fold growth like incremental folding or tectonic pauses. Condition (2) checks the consistency with a steady state process. The incision profiles deduced from T_0 and T_3 along the Bagmati section are quite similar (Figure 6). However, there seems to be a significant mismatch between the incision profiles on the northern limb of the fold. First, the wavelength of the incision profile is shorter for T_3 than for T_0. In addition, the similarity ratio of 0.195 ± 0.05 does not compare well with the ratio of their ages 0.24 ± 0.02. It thus appears that the conditions expressed by (1) and (2) are only approximately fulfilled. As expressed above, tectonic reasons for such a mismatch may be ruled out.

Instead, we invoke a model that accounts for river geomorphologic evolution, i.e., base level, gradient, and sinuosity changes. According to this model (see Appendix B for a more detailed description), the cumulative uplift $U(x, t)$ at point x since terrace formation at time t, with respect to a point attached to the Indian lithosphere just south of the MFT, can be written

$$U(x, t, t_i) = I(x, t, t_i) + D(x, t, t_i) + P(x, t, t_i). \quad (3)$$

Here $I(x, t, t_i)$ is the incision deduced from the elevation of the terrace tread i above the present river bed, $D(x, t, t_i) = D(x_0, t, t_i)$ represents the local base level change at the front of the fold since time t, relative to the Indian basement, i.e., the sedimentation rate [see also *Molnar et al.*, 1994], and $P(x, t, t_i)$ is the change in elevation at x due to possible changes of the river gradient and sinuosity. We neglect the role played by sea level changes and the contribution of deformation at the scale of the lithosphere (see Appendix B). $U(x, t, t_i)$ is thus only related to thin-skinned tectonic uplift.

Because the geomorphic contribution $P(x, t, t_i)$, climatically induced, is probably cyclic and thus bounded, the importance of P relative to the total incision will decrease with increasing terrace age. Let us assume, as a first approximation, that the average Holocene uplift rate is equal to the mean incision rate since T_0 formation, $u(x) \approx I(x, t, t_0)/(t - t_0)$. We focus on the youngest terrace T_3, in order to illustrate the role of the different geomorphic contributions. Equation (3) can be rewritten

$$\Delta I(T_3, x) = U(T_3, x) - I(T_3, x) = D(x, t, t_3) + P(x, t, t_3)$$

$$\approx I(x, t, t_0)\,\frac{(t - t_3)}{(t - t_0)} - I(x, t, t_3), \quad (3')$$

where $\Delta I(T_3, x)$ is the present deficit or surplus of incision since T_3 abandonment (Figure 7a). For the Bagmati and Bakeya Rivers this deficit reaches 5–10 m. It is greatest along the northern reach of the canyon (Figure 7a). The present deficit of incision could cause temporary aggradation on the back limb of the MFT fold (Figure 7b): the wide, braided channels of the Bagmati and Bakeya Rivers in the Chaura-Marin Dun may originate from this mechanism. Along the

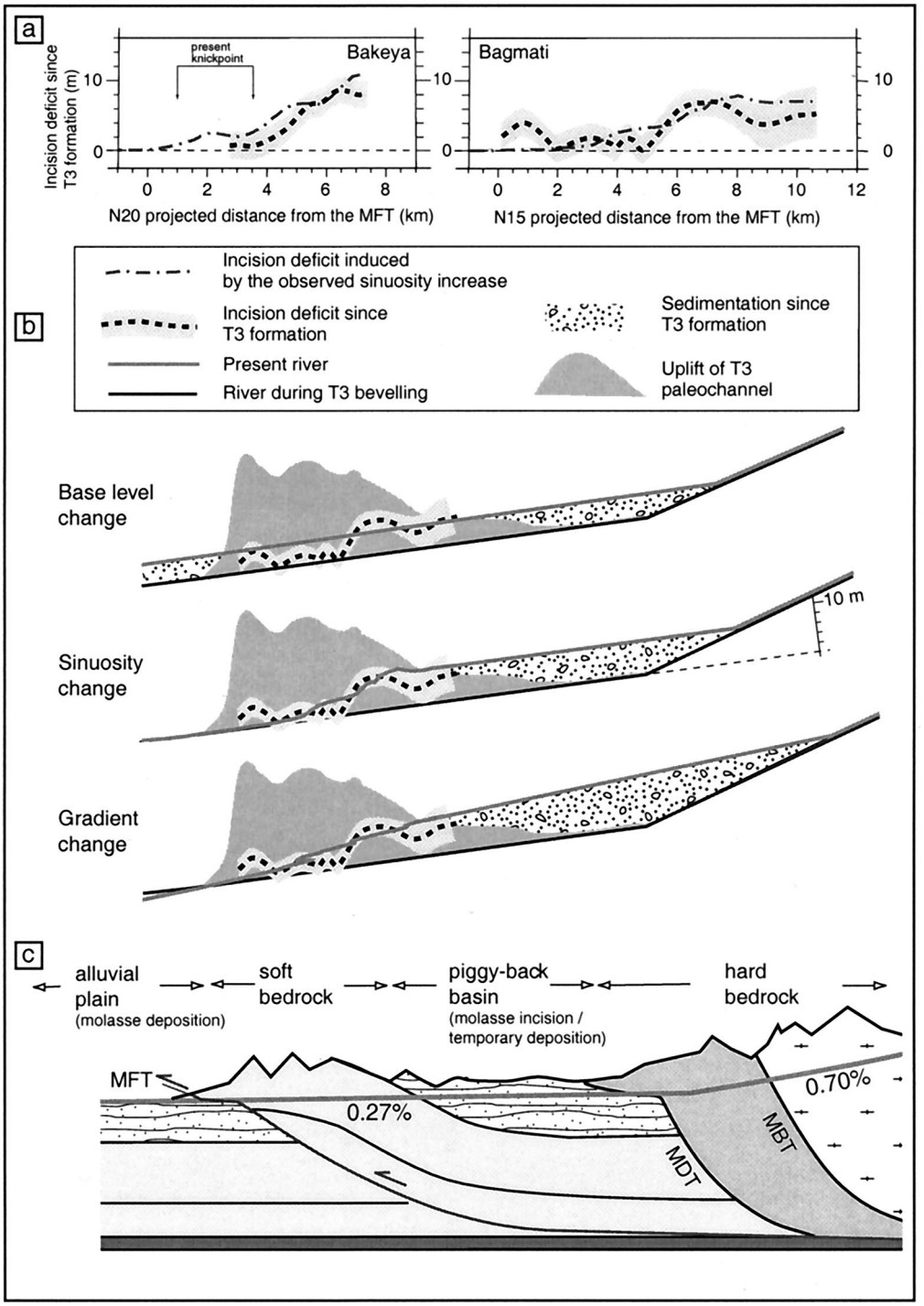

Figure 7. (a) Assuming that the incision profile since T_0 abandonment correctly mimics the long-term uplift rate, profiles of the incision deficit since T_3 (thick line) abandonment display common features along the Bagmati and Bakeya Rivers: a S shape and a deficit of 6–8 m on the back limb. (b) This deficit could have different origins: either a base level rise (i.e., a sedimentation pulse in front of the fold and across the fold), or a sinuosity increase mainly into the fold, or a general gradient increase. In these sketches, for clarity, the river is not scaled with the profiles of incision deficit and T_3 uplift, and the initial river is considered as a straight channel perpendicular to the fold axis. In the three cases the incision deficit would be associated to a temporary aggradation surface along the back limb of the MFT fold. (c) In the Bagmati valley the aggradation surface merges with the steeper northern reach of the river (slope of 0.7%) between the MDT and MBT.

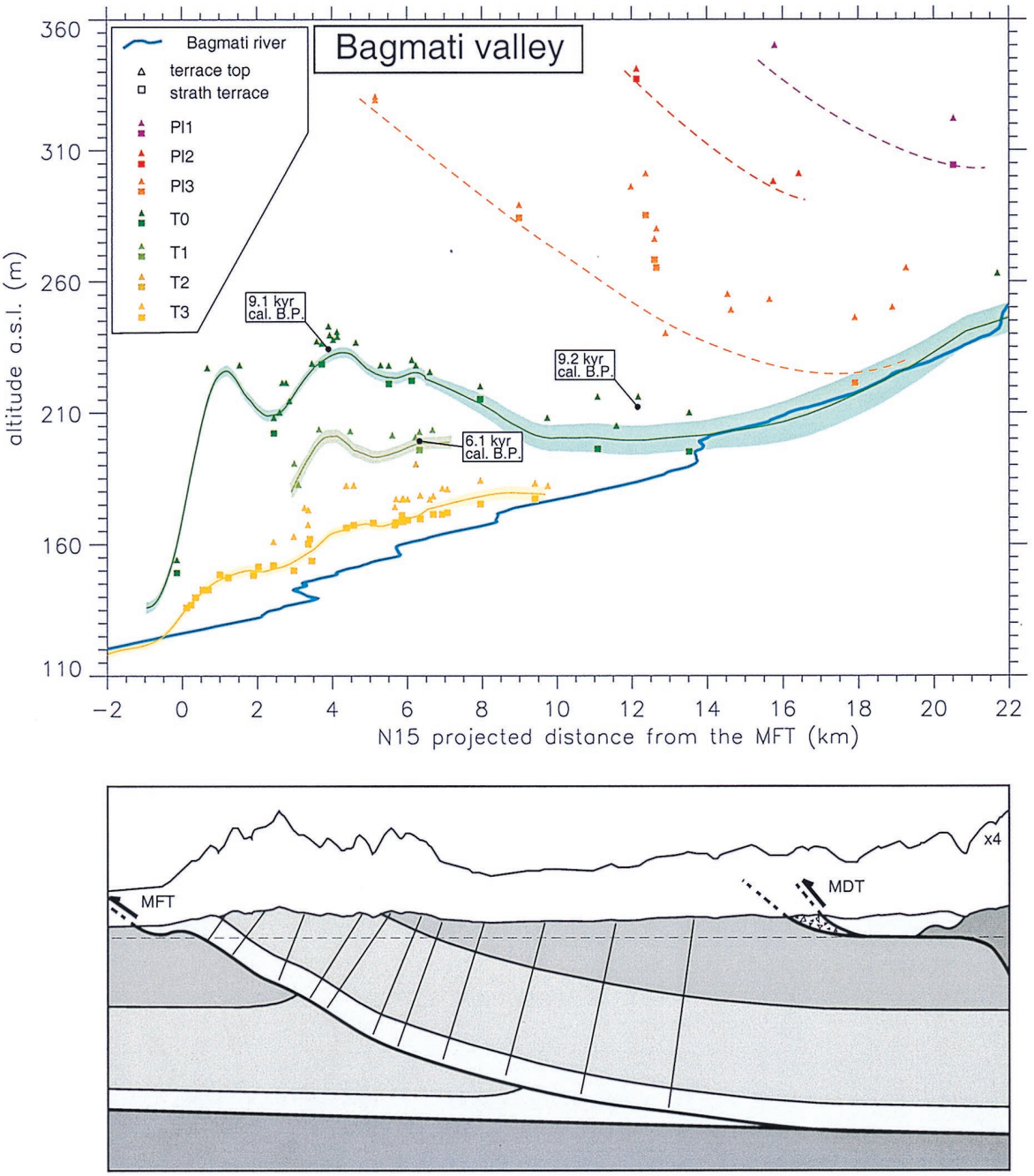

Plate 7a. (top) N15 projection of the strath terraces along the Bagmati River. The elevation of the strath levels computed from all DEM and field measurements (solid thin lines and dashed lines) are shown together with the individual field measurements. Solid thick lines correspond to Holocene terraces, and dashed lines correspond to hypothetical levels between late Pleistocene terraces presenting similar color and depth of weathering. (bottom) The structural cross section, with the same horizontal scale is shown for comparison. The terraces unambiguously attest to sustained Holocene and late Pleistocene activity of the MFT fold. In contrast, they did not record very significant offset across the MDT and suggest little deformation linked to this thrust.

Bakeya, a sharp increase of the incision deficit occurs just 3 km upstream of the center of the present knickpoint. This observation does not support the hypothesis of knickpoint retreat and the consequent diachronism in T_3 abandonment to explain the incision deficit. In section 4.2 we investigate base level, gradient, and sinuosity changes since the abandonment of the terraces as other possible causes for the observed incision deficits.

4.2. Estimation of Base Level Changes

There are no entrenched channels south of the MFT, and the common absence of red-weathered soils in that part of the

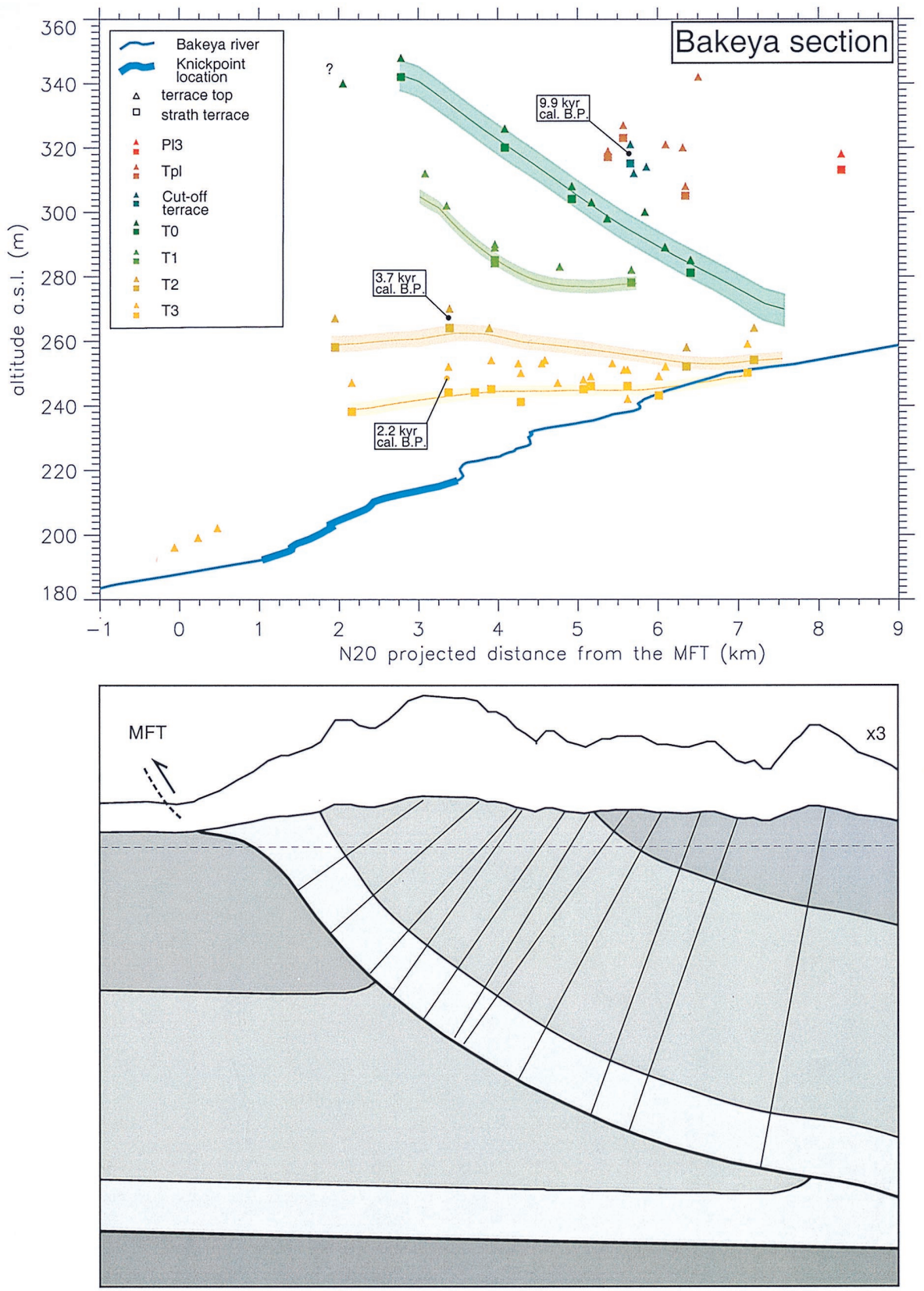

Plate 7b. Same as Plate 7a except for the Bakeya section. In the southern part of the section, the longitudinal profile of the river displays a 2- to 3-km-long gradient increase (thick blue line). As along the Bagmati River, the Holocene terraces attest to sustained activity of the MFT fold. Additionally, they show a greater incision in the southern part of the fold, where the ramp becomes steeper in the structural cross sections.

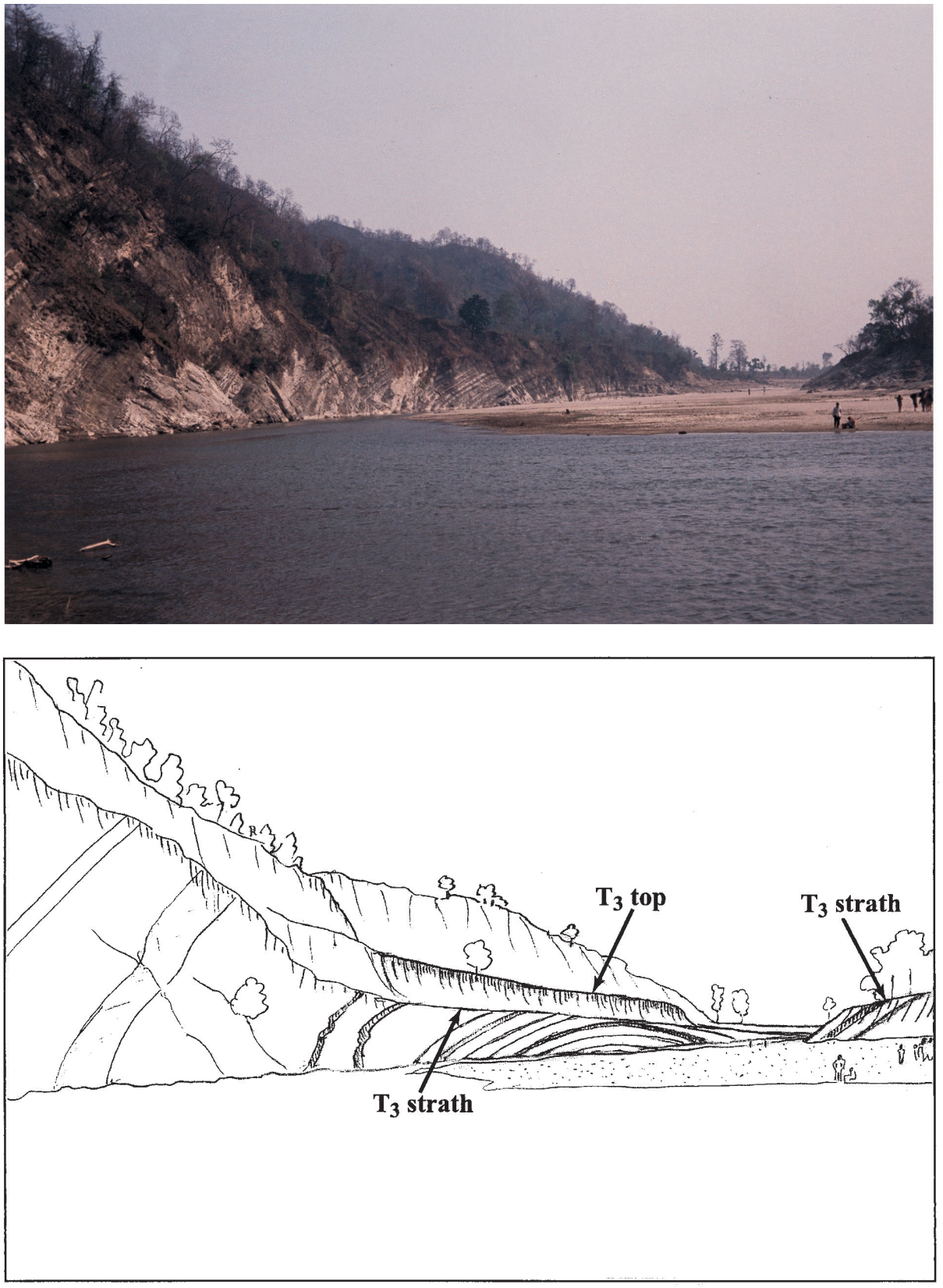

Plate 8a. (top) Southward view and (bottom) sketch of the T_3 terrace, where the Bagmati River leaves the gorge across the MFT fold and arrives in the Teraï. Note the clear strath level and regular 2- to 3-m-thick veneer of gravel. The terrace dips steeply to the south to merge with the modern floodplain of the Bagmati River in the Teraï.

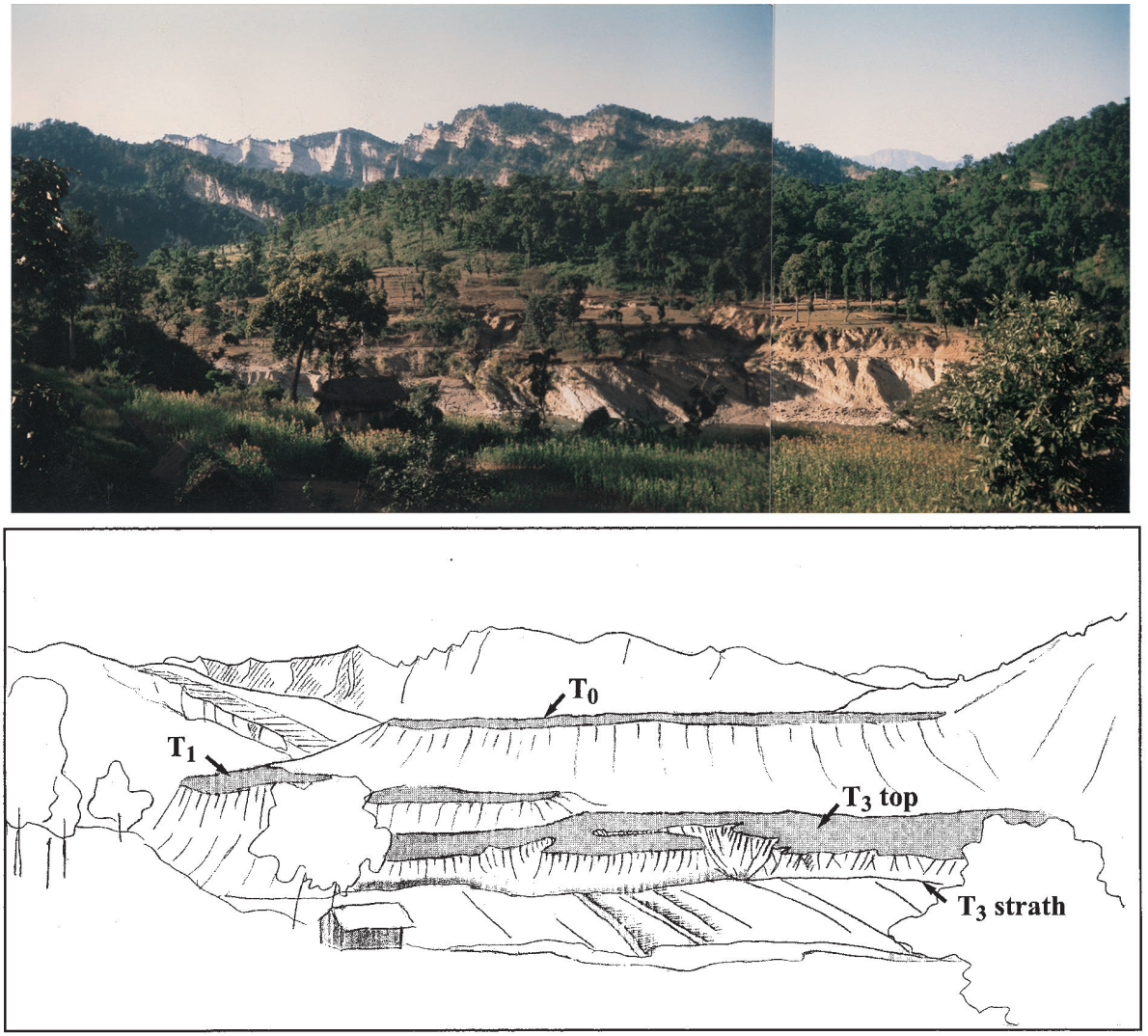

Plate 8b. (top) Westward view and (bottom) sketch of the two most prominent strath terraces, T_0 and T_3, along the Bagmati River. The view shows these terraces in the core of the MFT fold, where they lie at 90 and 30 m above the modern Bagmati River, respectively. The strath treads are beveled in Middle Siwaliks sandstones that strike N135°E and dip 30° to the north.

Gangetic Plain suggests that rivers aggraded during the Holocene. Some estimate of the sedimentation rate can be derived from the 2000-m thickness of the Upper Siwaliks in the geologic sections dated between 0 and 5 Ma according to magnetostratigraphy (Plate 4 and Figure 3). The absence of any visible angular unconformity suggests that these sediments were deposited before the onset of folding. We infer a minimum average sedimentation rate of 0.4 mm/yr. Hereafter, we assume a mean Holocene sedimentation rate in the foreland, just south of the MFT, of 0.4 ± 0.5 mm/yr. The large uncertainty accounts for the poor reliability of this estimate and probable climatic-induced variations.

Assuming this long-term sedimentation rate, a 1-m sedimentation may have occurred since T_3 abandonment. Even aggradation rates greater by 1 order of magnitude can not account for the shape and inflexion in the incision deficit profiles, observed in the Bagmati or Bakeya gorges (Figure 7b).

4.3. Estimation of Paleosinuosities

As shown in Figure 8a, an impression of river width and sinuosity during terrace beveling can be derived from the abundant terrace remnants along the Bagmati. Wide, flat Holocene terrace remnants, in particular at the level T_0 (Plates 6a, 6c, and 8b), indicate that at that time the active floodplain in the narrows was wider than the present one. In places, T_0 terraces are up to 400 wide. Given that the present floodplain of the Bagmati is wider in the Teraï or along the Chaura Marin Dun, such a wide floodplain would have been submerged during monsoonal floods. We therefore consider the terrace remnants to be representative of abandoned active floodplains. Three constraints can help to reconstruct the paleofloodplain corresponding to each terrace level. First, the paleofloodplain has to lie within the confines of the valley sides rising above the terrace level; second, it should encompass all terrace remnants

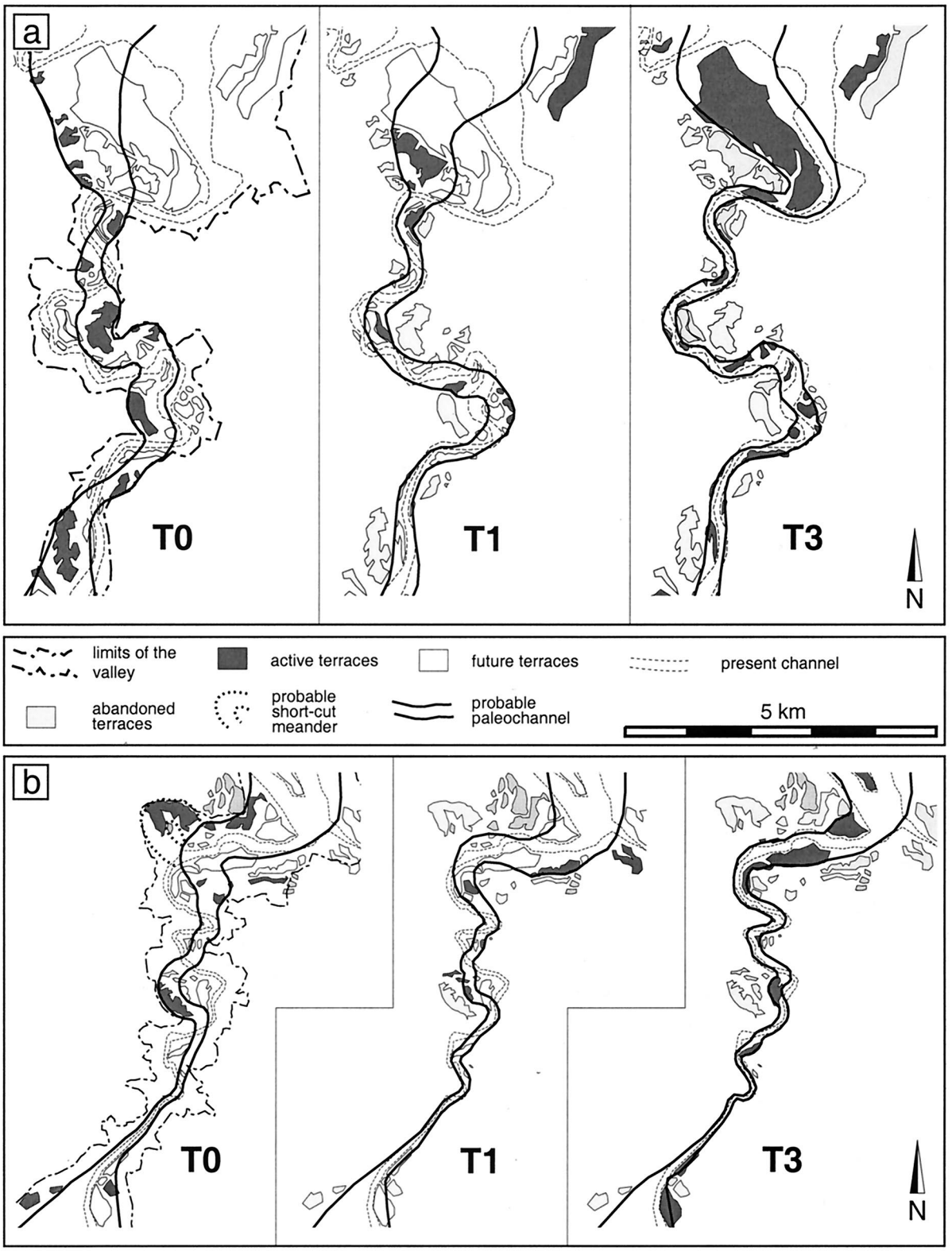

Figure 8. Reconstruction of the channel (bold solid line) at times of T_0, T_1, and T_3 beveling along (a) the Bagmati River and (b) the Bakeya River. Thin dashed lines delineate the modern floodplain. In each plot the terraces used to infer paleochannel geometry are dark shading. Past terraces (light shading) and future terraces (unshaded) are also shown. Paleochannels must lie within the confines of the valley sides rising above the terraces (heavy dashed line). Some terrace remnants attributed to tributaries such as the Marin Khola at the northern end of the canyon were not used in the reconstruction.

of a given level; and third, the radius of curvature and the wavelength of the meanders should be proportioned to the channel width, as observed for alluvial channels [*Leopold*, 1994] or for bedrock channels across the Siwaliks Hills (Figure ED3). Because the terrace remnants provide an incomplete record, they may be found consistent with various paleofloodplain geometries. The third condition was added in order to discard unrealistic channel paths. Paleofloodplain reconstructions corresponding to T_0, T_1, and T_3 are given in Figure 8a. Along the Bagmati narrows, the river was probably the widest (W = 300 m) and the least sinuous (1.8) at the time of T_0 abandonment (Table 2). For T_1 we obtain a width of 200 m and a sinuosity of 2.0. For T_3 a narrower width and more sinuous channel (2.1) are inferred, and the present riverbed shows the narrowest width and most sinuous channel (2.4) (Table 2). The sinuosity increase during Holocene times has caused an increase in channel length along the narrow. The resulting deficit of incision may be expressed by

$$\Delta I(T_3, x) = P(x, t, t_3) = S(x)[L(x, t) - L(x, t_3)], \quad (4)$$

where $L(x, t)$ is the longitudinal distance along the river at time t and $S(x)$ is the channel gradient, assumed constant. The sinuosity increase since T_3 abandonment accounts for both the shape and the amplitude of the incision deficit profile (Figures 7a and 7b).

Although the terraces are not as well preserved as along the Bagmati River, the paleochannel geometry can also be derived from the terrace remnants along the Bakeya River (Figure 8b). These reconstructions show a pattern similar to that observed along the Bagmati, with T_0 probably corresponding to the widest and least sinuous floodplain (Table 2). As for the Bagmati River, the sinuosity increase since T_3 abandonment matches correctly both the shape and the amplitude of the incision deficit profile (Figure 7a).

4.4. Estimation of Paleogradients

We are not aware of any way to assess changes of the river gradient during the Holocene. Strath terraces are indicators of temporary dynamic equilibrium [*Bull*, 1991] that may have been associated with different channel slopes depending on the fluvial regime at the time of their beveling. The principle of minimum stream power expenditure [*Chang*, 1988; *Yang and Song*, 1979; *Leopold*, 1994] implies that a river tends to establish a longitudinally constant energy slope. Given that along the short stream reach, considered here, water and sediment discharge do not vary significantly, this principle would imply a constant gradient. The modern Bagmati River has indeed a constant gradient of ~0.27%, where it flows across the molasse and soft bedrock lithologies exposed in the study area (Figure 7c).

The Holocene trend toward a dryer climate in this part of Asia may have forced hydrological modifications, including gradient increase due, for example, to a decrease of the sediment transport capacity of the rivers. Notably, an increase of the channel gradient by ~0.05% (20% change), since T_3 abandonment, may account for the incision deficit profile (Figure 7b). Such a mechanism would have induced incision in front of the MFT, as well as aggradation increasing upstream. However, the geometry of the channel south of the MFT and the constant thickness of the fill material on T_3 (Plates 7a and 7b) are not consistent with this interpretation. We therefore simply assume that during the Holocene the Bagmati River maintained a constant gradient equal to the gradient along the modern channel.

The geometry of the Bakeya River long profile is complicated by the presence of a knickpoint coinciding with the zone of highest incision rate (Figure 7b). This knickpoint may be tectonic in origin, similar to river long-profile convexities observed along the High Himalayan rivers [*Seeber and Gornitz*, 1983]. We will compensate the lack of information on the paleogeometry of the knickpoint by an increase of the uncertainty associated to $P(x, t)$.

4.5. Uplift Rates Along the Bagmati and Bakeya Rivers

Using (3) and the previous estimate of the nontectonic contributions, we derive for each terrace level an uplift rate profile (Plate 9) from the observed incision and measured terrace ages (Tables 1 and 2). The contribution of base level and sinuosity changes, computed from the parameters in Table 2, is shown in Appendix B (Figure B2). In this study, base level and sinuosity changes account for 5–10% of the uplift signal in the southern part of the narrows. However, these factors do significantly affect the upstream shape of the uplift profile because of sinuosity increase. As previously suggested, they affect much more the recent T_3 terrace than the older T_0 terrace. Although we now consider that $U(T_0)$ is different from $I(T_0)$, the previous discussion of the incision deficit since T_3 abandonment is still valid. Indeed, we verify that the uplift profiles for T_0 and T_3 (Plate 9a) are more similar than the incision profiles (Figure 6). The best similarity ratio for the uplift profiles ($U(T_3)/U(T_0)$ = 0.22) agrees better with the ratio of the age of abandonment of T_3 and T_0 (t_3/t_0 = 0.24) than the ratio derived from incision profiles ($I(T_3)/I(T_0)$ = 0.19) (Table 3).

Similar tests can be applied for the other terrace levels in the two valleys. The best fitting similarity factors between $U(x, T_1)$, $U(x, T_2)$ or $U(x, T_3)$ and $U(x, T_0)$ were computed according to a least squares criterion (Appendix D). The quality of the fit was assessed from the rms between the profiles scaled to $U(x, T_0)$ (Tables 3 and 4). It appears that the uplift curves are very similar and yield similarity factors close to those expected from the age ratios, by contrast with the incision profiles (Tables 3 and 4). We also use the Pleistocene terrace Pl_3 (Plate 6a) because the terraces of this family extend north of the fold where the constraints from the Holocene terraces are weak. For this terrace level we neglect the effect of sinuosity changes, which could not be estimated from the sparse terrace remnants. However, as explained previously, error should be moderate because of its older age. This terrace was not dated, but its age was adjusted in order to fit, on the southern remnant, the uplift rate as deduced from T_0 (Plate 9a). On the back limb, the uplift profile of the Pl_3 terraces, is also in good agreement with the uplift profile of T_0.

It turns out that the slightly different incision profiles derived from the various terraces along either the Bagmati or Bakeya Rivers can be reconciled with the same uplift rate profile once base level and sinuosity changes are corrected and assuming no gradient change. Note that the large uncertainties on the determination of base level changes and paleosinuosities are accounted for in the procedure used to retrieve tectonic uplift. Ignorance of these effects would have led to slightly biased results and unrealistically small uncertainties.

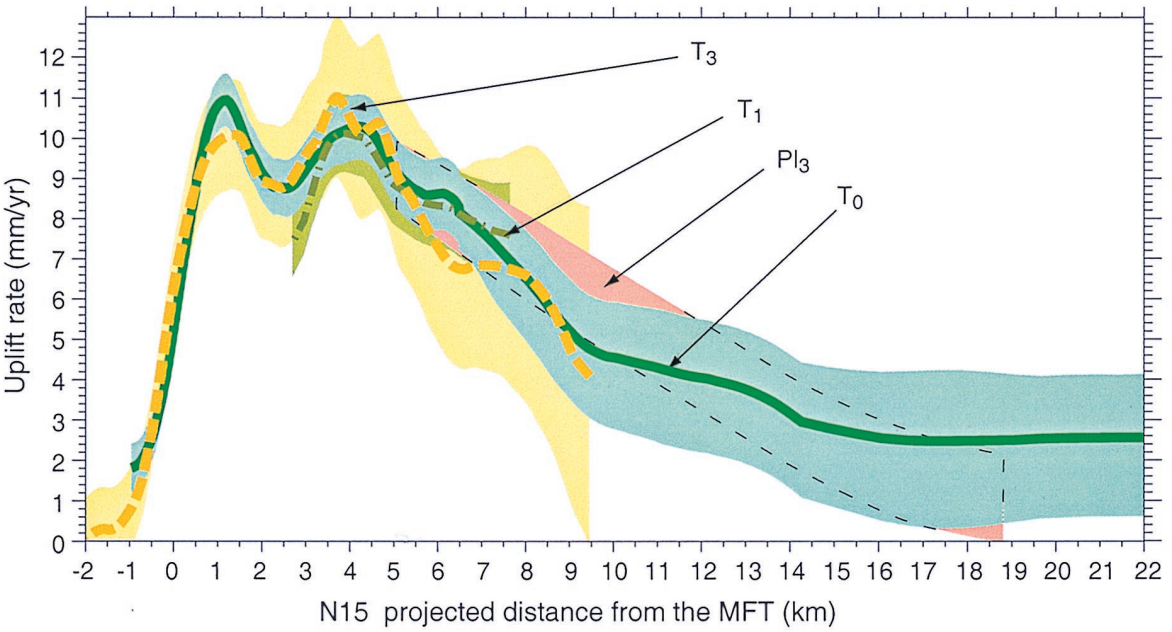

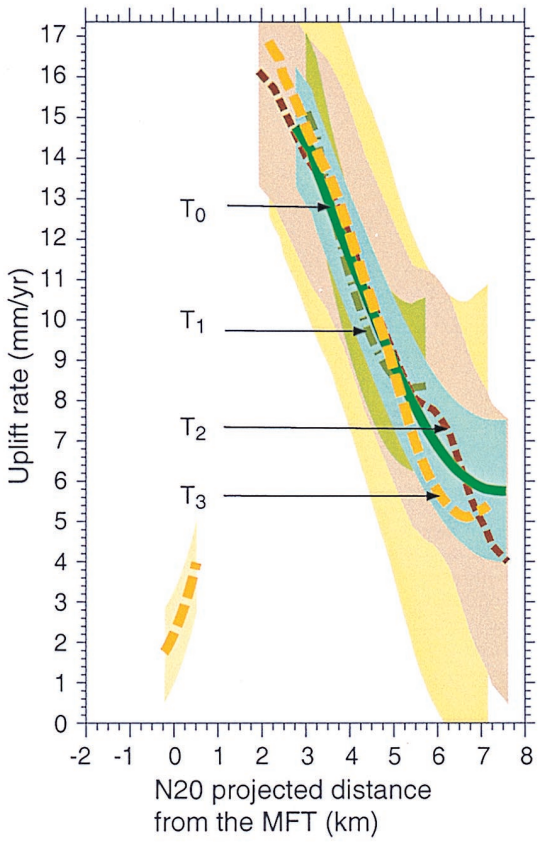

Plate 9. Comparison of uplift rate profiles deduced from the Holocene terrace levels along the (a) Bagmati and (b) Bakeya Rivers. Uplift rates were computed according to the terrace ages given in Table 1. Shaded area (delineated by dashed lines when in background) indicates the 1σ confidence interval on the mean profiles computed according to the procedure described in Appendix C. The different levels display uplift rate in closer agreement than the incision curves (Figure 6) on the back limb. The profile of the red-weathered terrace Pl_3 along the Bagmati River is shown for comparison. It was assigned an age of 22 ± 2 ka that provides the best agreement with the Holocene uplift rates deduces from the dated terraces.

Table 3. Comparison of Incision, Tectonic Uplift, and Age of T_1 and T_3 Terraces Along the Bagmati River, With Reference to T_0 Characteristics

	$I(T)/I(T_0)$	rms (I), m	$U(T)/U(T_0)$	rms (U), m	Age(T)/Age(T_0)
T_3	0.194 ± 0.005	14.4	0.22 ± 0.018	6.5	0.24 ± 0.02
T_1	0.607 ± 0.01	5.3	0.63 ± 0.043	2.5	0.660 ± 0.02

Ratios and rms were obtained by least squares adjustment as described in Appendix D.

5. Determination of Shortening Rate

5.1. Horizontal Shortening Deduced From Conservation of Mass

A simple way to deduce horizontal shortening from uplift profiles across the MFT fold is to assume conservation of mass. Let A be the area between the present profile of a fluvial terrace tread and the profile of the same terrace level at the time it was formed (Figure 9a). Let us assume, in keeping with the structural description above, that uplift across the MFT fold has resulted from horizontal sliding of a unit with thickness h detached from the basement (Figure 9a). Assuming plane strain and conservation of mass, we get that the mean horizontal displacement d, necessary to account for the deformation of the terrace, is

$$d(t, t_i) = A(t, t_i)/h = \left(\int_{x=0}^{x_M} U(x, t, t_i)\, dx \right) / h(x_M). \quad (5)$$

For application, this approach requires a continuous terrace tread across the growing fold. The only such terrace is the T_0 level along the Bagmati River. Deformation of that level corresponds to an area of $A(t, t_0) = 1.05\ (+0.25/-0.3)$ km^2. According to the structural description above, the depth of the basement is 5.0 ± 0.3 km beneath the MFT and dips northward with a slope of 2.5%. Given that the MFT ramp merges with the décollement ~18 km north of its trace at the surface, the depth to the décollement beneath the fold is 5.5 ± 0.3 km. We get a shortening $d(t, t_0) = 192$ m ± 60 m since 9.2 ± 0.2 cal ka. We infer a shortening rate of 21 ± 7 mm/yr.

5.2. Horizontal Shortening Determined From a Model of Fault-Bend Folding

Casual inspection of Plate 7 suggests that the uplift profiles recorded by the Holocene terraces are related to the geological structure of the fold. Indeed, the 3-km wavelength of the uplift rate in the middle of the fold seems to correlate with variation of the dip of the ramp at depth, as inferred from the bedding dip angles at the surface in the Bagmati gorge. Along the Bakeya, the steeper bedding dip angles imply a steeper ramp than along the Bagmati section. The resulting narrower fold zone deduced from the balanced section would account for the narrower zone of active uplift. The correlation between structural geology and recent uplift is, in fact, expected for a fault bend fold. Indeed, according to this model the hanging wall accommodates deformation imposed by the fault geometry at depth by bedding plane slip with no change of the length and width of the beds (Figure 19b). It follows that on the back limb, uplift rate on a fault bend fold depends on the dip of the fault at depth, which is equal to the bedding dip. In that case the local uplift since time t_i, $U(x, t, t_i)$, related to an increment of horizontal shortening $d(t, t_i)$, must obey

$$U(x, t, t_i) = d(t, t_i) \sin \theta(x), \quad (6)$$

where $\theta(x)$ is the dip angle at point x. This equation assumes cylindrical geometry. In fact, the geological maps show that strikes can slightly deviate from the general N105°E direction of the fold axis, suggesting that the ramp at depth may locally be oblique, to the mean fold axis (Plates 1, 6a, and 6c). In order to account for these deviations, (6) must be modified to

$$U(x, t, t_i) = d(t, t_i) \sin \theta'(x), \quad (7)$$

where

$$\theta'(x) = \operatorname{atan} [\sin \rho(x) \tan \theta(x)], \quad (8)$$

and $\rho(x)$, as defined by *Apotria et al.* [1992], represents the angle between the particle trajectory on the oblique ramp and the strike of this ramp. It is defined by

$$\sin \rho(x) = \cos \theta(x) \sin [\phi(x) - \phi_0] / \{1 - [\sin \theta(x) \sin (\phi(x) - \phi_0)]^2\}^{1/2}, \quad (9)$$

where $\phi(x)$ is the azimuth of the bedding strike at point x and ϕ_0 is the regional mean direction of transport, taken perpendicular to the mean fold axis (N15°E). The N15°E direction corresponds to the stretching lineation in the higher Himalaya [*Brunel*, 1986] and is roughly perpendicular to the trend of the Himalayan arc in central Nepal. After simplification, (7) becomes

$$U(x, t, t_i) = d(t, t_i) \sin \theta(x) \sin [\phi(x) - \phi_0]. \quad (10)$$

To test this prediction, we have compared dip angles with tectonic uplift along the Bagmati and Bakeya Rivers. The values of $\sin \theta'(x)$ obtained from the bedding dip measurements along the Bagmati and Bakeya sections are shown in Figures 10a and 11a. The data are scattered but a mean profile can be constructed the same way as for terrace treads (Appendix A). The confidence interval on this profile was obtained by assigning uncertainties of 10° on strike measurements and 3° on dip measurements. The procedure used to compute the resulting

Table 4. Same as Table 3 Except for the Bakeya River

	$I(T)/I(T_0)$	rms (I), m	$U(T)/U(T_0)$	rms (U), m	Age(T)/Age(T_0)
T_3	0.19 ± 0.003	23.8	0.24 ± 0.04	6.5	0.24 ± 0.02
T_2	0.37 ± 0.014	9.7	0.40 ± 0.05	3.3	0.40 ± 0.02
T_1	0.66 ± 0.018	4.0	0.66 ± 0.06	4.3	0.66 ± 0.02

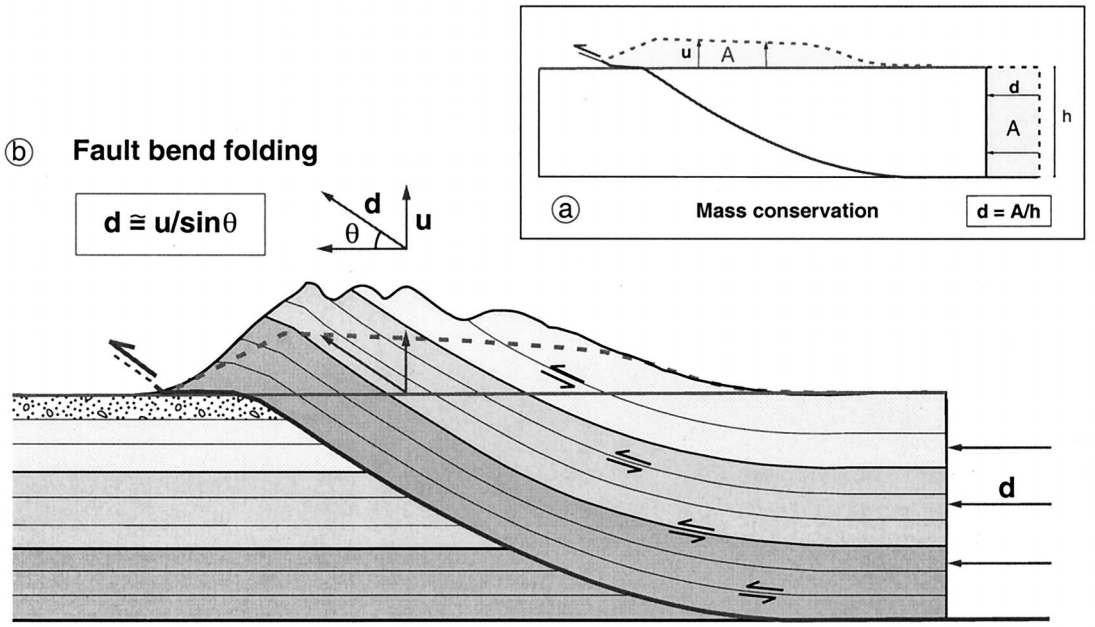

Figure 9. Sketch showing two ways of computing horizontal deformation d from incremental folding of a terrace level. (a) We simply assume mass conservation. A continuous terrace level is required and some constrain on the depth of the basal décollement, h. (b) If fault bend folding is assumed, the structural uplift is simply proportional to the sine of the local bedding dip angle and to the horizontal shortening, as indicated by equation in inset.

uncertainty is expressed by equation (C1) (in Appendix C). Short wavelengths ($\lambda < 1$ km) in the mean profiles were filtered out. Figures 10b, 10c, 11b, and 11c show that sin θ' and the tectonic uplift obtained from terraces T_0 and T_3 are proportional, as predicted by (7). We deduce that 196.5 ± 10.5 m of horizontal shortening has occurred since the abandonment of terrace T_0 along the Bagmati River and 44.5 ± 4 m since the abandonment of T_3.

The amount of shortening deduced from all the terraces along the Bagmati and Bakeya Rivers are listed in Table 5. When these values are plotted as a function of the age of abandonment of the terraces (Figure 12), it indicates a rate of horizontal shortening of 20.4 ± 1 mm/yr during the Holocene period.

5.3. Discussion of Uncertainty

The two determinations above are consistent but are associated with very different uncertainties. The 30% uncertainty associated with the estimate based on conservation of mass is essentially due to the uncertainty on the depth to the basement and to the poor control on tectonic uplift on the northern limb of the fold. This poor control is related to higher uncertainties on the strath measurements along this reach and on the contribution of sinuosity changes to river incision.

The estimate of the shortening rate based on the fault bend model is much better constrained (see Appendix D for the procedure used to compute uncertainties). Taking into account the structural information all along the gorges, this model provides several independent estimates of the cumulative shortening and allows an efficient reduction of errors, below 10%, for each terrace profile (Table 5). This reduction of errors is acceptable provided that the terrace treads can be considered as isochrons. Moreover, this model provides additional constraints on the estimate of the shortening rate by considering several terrace levels. Although we obtained seven independent estimates of shortening, only four independently dated treads were included in the computing: T_0 (SIW54, SIW40) and T_1 (SIW47) along the Bagmati River and T_2 (NE-3) and T_3 (NE-2) along the Bakeya River (Table 2).

It should be noted that in both approaches the shortening rate is a mean value over the Holocene that neglects the seismic cycle. In fact, the fold at the MFT must have grown by coseismic increments rather than continuously over the Holocene. The shortening rate deduced from the least squares fit in Figure 12 might actually be slightly biased. Some interseismic deformation $c(t)$ may not have been released yet, and some interseismic deformation $c(t_i)$ may not have been released at the time t_i of abandonment of terrace T_i. In that case, the amount of horizontal shortening $d(t, t_i)$, expressed in the deformation of terrace T_i, is

$$d(t, t_i) = c(t) - c(t_i) + a(t - t_i), \tag{11}$$

where a is the long-term average shortening rate.

The term $c(t)$ may be seen as a random variable with values in the range between zero and the typical seismic slip during the large magnitude 8 earthquakes that are thought to activate the MFT fold. In keeping with the estimated coseismic slip of large Himalayan earthquakes [*Molnar and Deng*, 1984; *Pandey and Molnar*, 1988; *Seeber and Armbuster*, 1981], we set this value to 5 m. Accounting for the uncertainty on each $c(t_i)$, the slip rate is constrained between 19.5 and 22.5 mm/yr at the 68% confidence level, with a most probable value of 21 mm/yr. The introduction of possible discrete growth of the MFT fold leads to a small increase in the shortening rate of 0.5 mm/yr and to a larger uncertainty, compared with the former assumption of continuous growth.

The shortening rate computation and more particularly the associated low-level uncertainty are clearly dependent on our

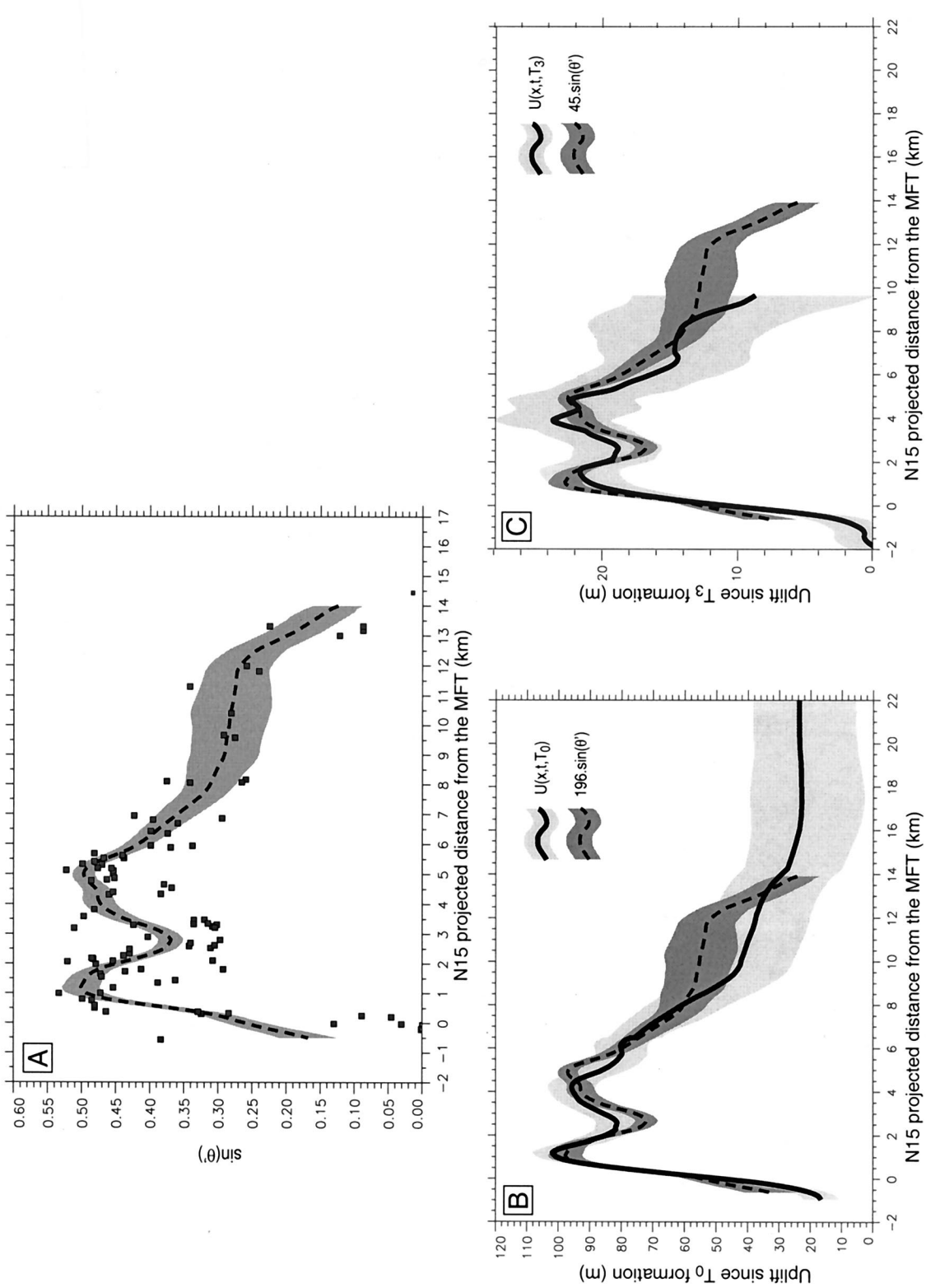

Figure 10. Test of fault bend fold model along the Bagmati section. (a) Sine of bedding dip angles (according to equation (10)) along the Bagmati River. The mean profile, computed following procedure described in Appendix A, is shown with its 1σ confidence interval. A 10° uncertainty was assigned to strike measurements and 3° to dip angle measurements. (b and c) As predicted by the fault bend model, this profile is shown to be proportional to the profiles of uplift deduced from terrace T_0 and T_3. Accordingly, we deduce that 196.5 ± 10.5 m of horizontal shortening has occurred since T_0 abandonment and 44.5 ± 4 m since T_3 abandonment.

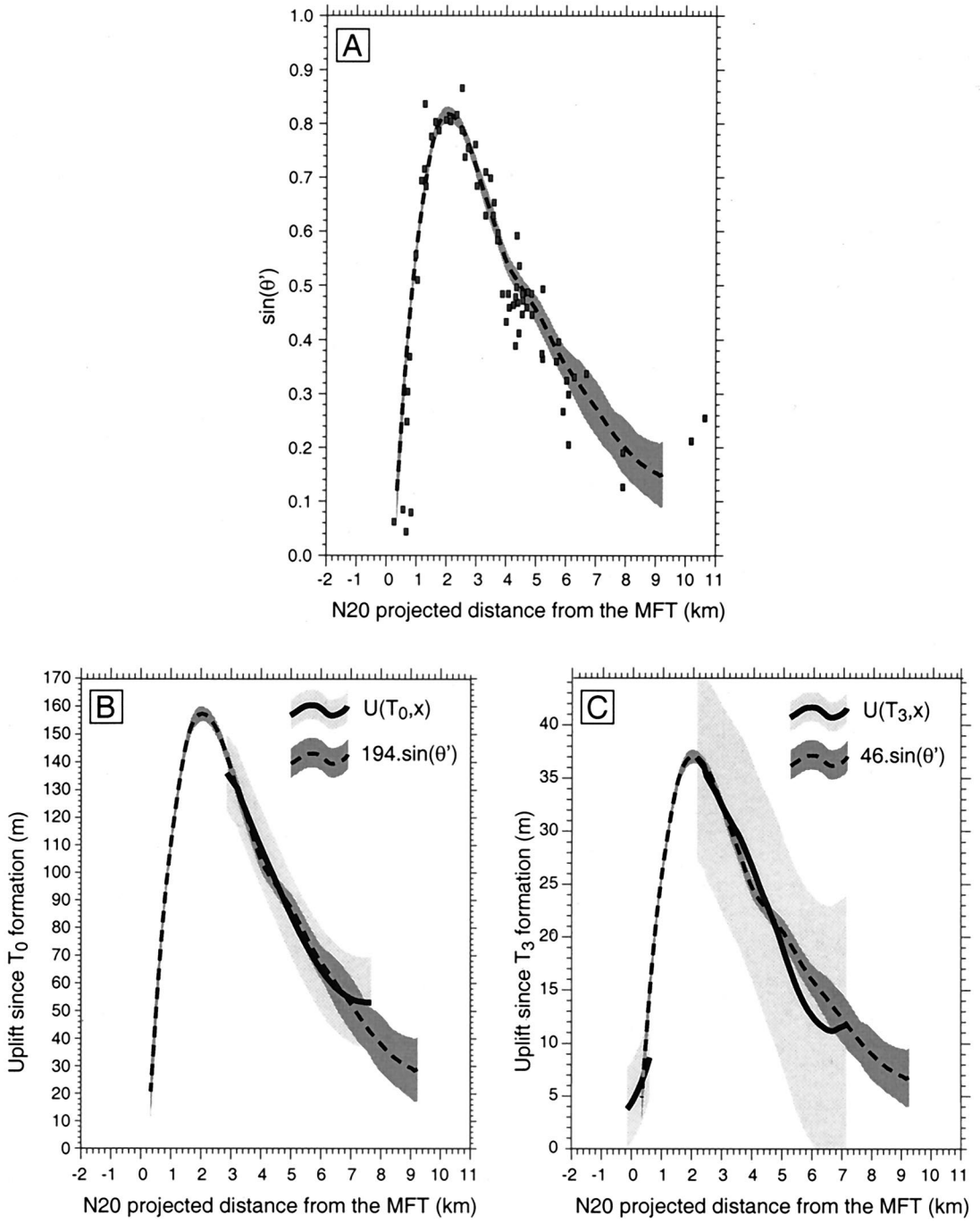

Figure 11. Same as Figure 10 for the Bakeya section. We infer 194 ± 15 m of horizontal shortening since T_0 abandonment, and 46 ± 8 m since T_3 abandonment.

two main hypothesis: the terrace treads represent isochrons with ages within the bounds derived from the ^{14}C samples, and the steady state fault bend fold model is relevant to explain terrace deformation. In the framework of these two hypothesis, the shortening rate is finally 21 ± 1.5 mm/yr.

6. Seismotectonic Implications

Several estimates of the rate of shortening across the central Himalaya have been previously obtained. One estimate is based on the sedimentological record in the Indo-Gangetic foredeep. Well data indicate that proximal facies have migrated southward during sedimentation [*Karunakaran and Ranga Rao*, 1979; *Sastri*, 1979; *Sastri et al*., 1971]. Assuming southward migration of a steady state accretionary prism, *Lyon-Caen and Molnar* [1985] deduced an average thrusting rate of 10–15 mm/yr over the last 10–20 Myr. In their study of the south Tibetan graben, *Armijo et al*. [1986] obtained a shortening rate across the Himalaya of 20 ± 10 mm/yr. From their estimation of the seismic moment tensors for the large earthquakes of this century, *Molnar and Deng* [1984] inferred a value of 18 ± 8 mm/yr. More recently, *Bilham et al*. [1997] reported Global Positioning System (GPS) measurements collected be-

Table 5. Shortenings Since Abandonment of the Various Holocene Terraces

	Bagmati Valley [0, 12 km]		Bakeya Valley [2, 8 km]	
	Shortening $d(t)$, m	rms, m	Shortening $d(t)$, m	rms, m
T_0	196.5 ± 10.5	6.5	194 ± 15	5.0
T_1	123 ± 9	5.0	130 ± 13.5	3.5
T_2			75 ± 11.5	1.9
T_3	44.5 ± 4	1.5	46 ± 8	1.8

The rms criterion expresses the fit between terrace uplift and theoretical fault bend folding curve from the computation of the standard deviation of $g(x) = [U(x, t) - d(t) \sin \theta'(x)]$, along the N15 profiles from x_1 to x_2 $[x_1, x_2]$ (Appendix D).

tween 1991 and 1995 that indicate 17.7 ± 2 mm/yr of horizontal contraction in the Himalaya of Nepal. Elastic dislocation modeling of the horizontal GPS data together with vertical leveling data led these authors to infer that the Main Himalayan Thrust fault (MHT) is locked south of the High Himalaya and that northward it connects a creeping fault in the middle crust slipping at 20 ± 3 mm/yr. These various approaches are not directly comparable since they do not consider the same time span, but they all provide estimates similar to the shortening rate across the MFT obtained in this study. It suggests that at the longitude of Kathmandu, localized thrusting along the MFT accounts for nearly all the shortening across the Himalayas.

Along the Himalayan arc, four earthquakes with magnitude 8–8.5 occurred over the last century. *Seeber and Armbuster* [1981] suggested that these earthquakes ruptured the décollement ahead of the Higher Himalaya up to the most frontal structures in the sub-Himalaya and farther south. Such an interpretation of southward rupture propagation is consistent with the extent of the damage reported for the 1934 Bihar Nepal earthquake [*Pandey and Molnar*, 1988; *Chander*, 1989]. None of the $M_w \geq 8$ large Himalayan earthquakes is known to have produced surface breaks that would provide evidence for this interpretation. The frequent earthquakes of magnitude 7 generally take place in a narrow band just north of the High Himalaya [*Ni and Barazangi*, 1984]. Strong motion data from the 1991 M_s 7.1 Uttarkashi earthquake suggest that this earthquake nucleated at the front of the High Himalaya and activated the basal décollement beneath part of the Lesser Himalaya [*Cotton et al.*, 1996]. In central Nepal, leveling data and seismic monitoring over the last decade indicate intense microseismicity (Figure 1) and strain and stress buildup at the front of the High Himalaya [*Jackson et al.*, 1992; *Jackson and Bilham*, 1993; *Bilham et al.*, 1997; *Pandey et al.*, 1995]. It has been recently proposed that this strain accumulation is located at the tip of a creeping dislocation [*Bilham et al.*, 1997] and plastically absorbs a fraction of the long-term shortening rate across the range. Accordingly, the topographic front of the High Himalaya would result from the cumulative expression of the interseismic deformation.

By contrast, our terrace study implies that this interseismic

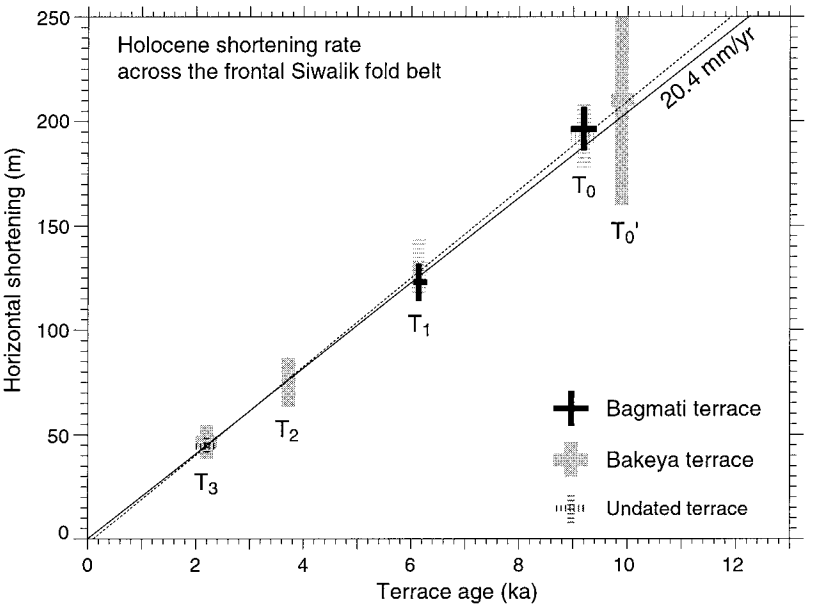

Figure 12. Plot of horizontal shortening deduced from the various dated terrace treads along the Bagmati and Bakeya section as a function of age of terrace abandonment. These data are consistent with a uniform 20.4 ± 1 mm/yr shortening rate over the Holocene period (solid line). The sample SIW-07 found in the abandoned meander T_0' provides an additional date but the associated shortening does not constrain the convergence rate. The other undated terraces, assuming the same age of the equivalent level in the other valley, are in close agreement with the obtained regression line. However, they have not been taken into account for the computation of the shortening rate. If the fold is assumed to have been growing by incremental deformation during large earthquakes, the mean shortening rate is slightly modified. Indeed, some amount of elastic strain at the large scale may yet remain to be released or may not have been released at the time of formation of the different terraces. Assuming that these increments can be as large as 5 m of horizontal shortening and that all values between 0 and 5 m are equally probable, we get that the long-term averaged shortening rate, that fits the terrace record best, is 21 ± 1.5 mm/yr (dashed line).

straining is essentially elastic since, on the long term, it must be transferred to the MFT in the foothills. As proposed by *Pandey et al*. [1995], we suggest that strain and stress build up around a midcrustal ramp during the interseismic period and this elastic deformation would be essentially released and transferred to the most frontal structures during the large earthquakes. The accumulated upheaval seen in leveling data must be partly relaxed when large earthquakes activate the décollement beneath the Lesser Himalaya. We thus interpret the topographic front of the High Himalayas to have resulted from passive overthrusting on the midcrustal ramp that is inferred to connect the flat décollement beneath the Lesser Himalaya (Figure 2). According to this seismotectonic model and to previous studies [*Ni and Barazangi*, 1984; *Seeber and Armbruster*, 1981], Himalayan earthquakes may nucleate at the ramp-flat transition and may relax the elastic strain accumulated around the locking zone during the interseismic period. These earthquakes may activate only a fraction of the flat beneath the Lesser Himalaya, with magnitudes of around 6–7, such as the Uttarkashi event. The whole flat, up to the MFT in the southern foothills, would be only activated during the $M > 8$ major events. Despite no evidence of surface rupture along the MFT, we may therefore assume that the growth of the MFT fold is only due to the repetition of large magnitude 8–8.5 earthquakes, such as the Bihar-Nepal earthquake that struck eastern Nepal in 1934. These major earthquakes account for most of the India–south Tibet convergence and therefore would be much more efficient in transferring slip than smaller events.

7. Conclusions

This study illustrates that geomorphic and structural investigations concur to provide tight constraints on fold growth. We show that in deriving tectonic uplift from river incision, one has to be careful about the possible contribution of base level, gradient, and sinuosity changes. In the present case these terms amount to only a small fraction of river incision. It must be realized that in a quieter tectonic setting, river incision may mostly result from these effects. The introduction of these refinements in the model allows correction of a small bias and, more importantly, an explicit account in the computation of uncertainties for the poor control on the initial geometry of the terraces. The use of a fold model, based on structural data, appears to be an efficient way to reduce uncertainties in the determination of horizontal shortening from tectonic uplift, based on geomorphic data such as fluvial terraces.

Our geomorphic analysis shows that the MFT is the only active structure south of the Lesser Himalaya in central Nepal. Over the Holocene it has absorbed on average 21 ± 1.5 mm/yr of N-S shortening. The 1.5 mm/yr uncertainty defines the 68% confidence interval that accounts for the uncertainties in the determinations of age and shortening and for incremental fold growth. Thrusting on the MFT seems to absorb most of the shortening rate across the whole Himalaya. The comparison of our data with recent seismic and geodetic studies suggests that present interseismic deformation is stored elastically and will be released by the next large ($M_w > 8$) earthquake. Such a large earthquake probably breaks the main Himalayan thrust fault from below the High Himalaya to the near surface at the front of the Himalayan foothills and results in incremental activation of the MFT.

Appendix A: Building of a Continuous Terrace Profile From Isolated Remnants

In this appendix we describe the procedure that we have applied to interpolate elevations between isolated terrace remnants to yield continuous strath terrace profiles along the various river reaches that we surveyed. Such an exercise makes sense only if the terrace remnants were correctly associated on the basis of their alluvial veneer characteristics and respective elevations above the modern river channel. Given the 10-km width of the fold and the 5-km depth to the décollement, we consider that the observed thin-skinned tectonics produced wavelengths larger than a few kilometers. We therefore use a 2.5-km-wide sliding window. For a given position of the window the elevations are adjusted with a parabolic curve. A weighted least squares criterion is minimized. Data are weighted according to their assigned 1σ uncertainties. Elevations measured with a digital altimeter (Pretel altimeter) are assigned a 3-m uncertainty after barometric correction. We also used elevations measured with a Tomen altimeter that were assigned a 1σ uncertainty of 5 m. Elevations measured from the digital elevation model were corrected from the estimated thickness of the gravel overlying the strath and assigned an uncertainty of 18 m, accounting for nominal uncertainty of the DEM (15 m) and the contribution of gullies or trees on the terrace. From the autocorrelation function of the DEM we estimate that measurements three pixels apart can be considered as independent. We used all the values on the DEM grid but assigned them an uncertainty 3 times larger than the 18-m standard uncertainty. The point at the center of the 2.5-km sliding window is then ascribed the value predicted by the parabolic curve. When terrace treads are >2.5 km apart, the size of the sliding window is increased so that at least three terrace treads are covered. The final curve is then smoothed by suppressing wavelengths <1 km. It yields the most probable elevation profile $z(x)$ of the considered strath level. Because we are projecting three-dimensional terrace measurements on a vertical cross section and thus smoothing the profile, local altimeter measurements may differ by >3 m from the final profile (our a priori error). The same procedure is used to compute a continuous profile from the dip angle measurements.

Appendix B: Relating Tectonic Uplift and Incision

B1. Principles

Retrieving tectonic deformation from isochronous straths requires a hypothesis about initial geometry of the terraces at the time of their formation. A convenient and straightforward hypothesis is to assume that the straths were initially similar to the modern channel. Accordingly, the incision, measured from the difference in elevation between the terrace remnants and the modern river bed, is considered as a proxy for tectonic uplift [*Iwata et al*., 1984; *Molnar*, 1987; *Rockwell et al*., 1984; *Burbank et al*., 1996]. If the various terrace levels have developed at times of fluvial regimes different from the present, change of the river geometry may have occurred and must be accounted for, since they can be sources of differential incision not related to uplift.

In this appendix we propose some equations to relate tectonic uplift and river incision by taking account of possible change of river geometry. $T(x, t)$ and $R(x, t)$ refer to the

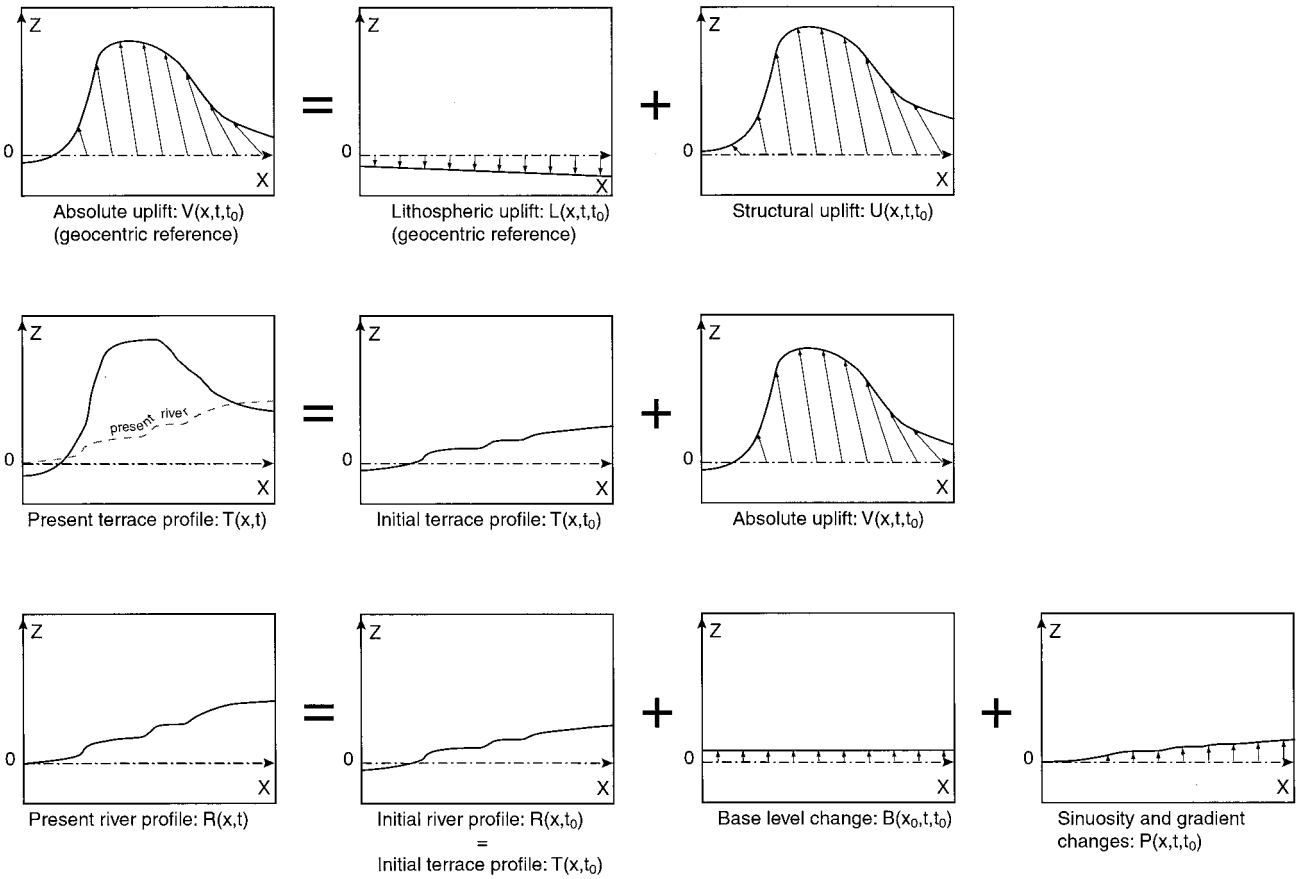

Figure B1. Diagram describing the various contributions to the elevation profile of a terrace level $T(x)$. Functions $V(x)$, $L(x)$, $T(x)$, $R(x)$, and $B(x)$ are expressed with respect to a geocentric reference frame.

terrace profile and the river profile, respectively, at time t. At the time t_i of the abandonment of the strath, T_i, the strath and river profiles coincide $T(x, t_i) = R(x, t_i)$. At a present time t, the terrace profile relates to the initial geometry according to (Figure B1)

$$T(x, t) = T(x, t_i) + \left(1 + \frac{S(x)}{\tan \theta(x)}\right) V(x, t, t_i) = R(x, t_i) + \left(1 + \frac{S(x)}{\tan \theta(x)}\right) V(x, t, t_i), \quad \text{(B1)}$$

where $V(x, t)$ is the absolute uplift relative to the geoid, $S(x)$ is the channel slope, and $\tan \theta(x)$ is the ratio (vertical uplift/horizontal shortening). Except for steep mountainous streams, the term $S(x)/[\tan \theta(x)] \ll 1$ can usually be neglected. For the Bagmati and Bakeya Rivers, a posteriori computation shows this term is of the order of 0.6%. In the following, only vertical displacements along a profile are considered.

Absolute rock uplift can be retrieved provided that $R(x, t_i) = T(x, t_i)$ can be expressed in a geocentric reference frame. If we consider a terrace tread that would extend linearly far from the zone of tectonic uplift, the undeformed treads provide a local reference frame allowing for the computation of a "structural uplift," $U(x, t, t_i)$. Given that the MFT is thought to mark the southern extent of thin-skinned deformation in the sub-Himalaya, we may, for example, consider a reference point attached to the subsiding Indian lithosphere. In that case, structural uplift corresponds to rock uplift in the reference frame of the Indian basement. If $L(x, t, t_i)$ expresses the regional vertical displacement of the Indian lithosphere, we may write (Figure B1)

$$V(x, t, t_i) = L(x, t, t_i) + U(x, t, t_i). \quad \text{(B2)}$$

Let us now consider the river profile. It may be written

$$R(x, t) = R(x_0, t) + \int_{l(x_0)}^{l(x)} S(l, t)\, dl, \quad \text{(B3)}$$

where x_0 lies just south of the MFT, and $S[l(x), t]$ is the stream gradient expressed as a function of the along-stream curvilinear distance from the point at the MFT outlet.

The change in the river profile over the period $[t_i, t]$ is then (Figure B1)

$$R(x, t) - R(x, t_i) = R(x_0, t) - R(x_0, t_i) + \delta\left(\int_{l(x_0)}^{l(x)} S(l, t)\, dl\right) = B(x_0, t, t_i) + P(x, t, t_i). \quad \text{(B4)}$$

The first term $B(x_0, t_i, t)$ reflects the base level change in a geocentric reference frame, which depends on the lithospheric uplift $L(x_0, t, t_i)$ and on sediment accumulation $D(x_0, t, t_i)$,

$$B(x_0, t, t_i) = D(x_0, t, t_i) + L(x_0, t, t_i). \quad \text{(B5)}$$

The second term $P(x, t, t_i)$ in (B4) expresses the elevation changes induced by the changes of the river geometry. Let us

now relate the curvilinear distance $l(x)$ to the average river sinuosity between x and x_0, $s(x, x_0)$,

$$l(x) = x, s(x, x_0). \quad \text{(B6)}$$

Equations (B3) and (B4) can then be written

$$R(x, t) = R(x_0, t) + \int_{x_0}^{x} s(u, t)S(u, t)\, du, \quad \text{(B7)}$$

$$P(x, t + \Delta t) = \int_{x_0}^{x} s(u, t)\Delta S(u, t)\, du + \int_{x_0}^{x} \Delta s(u, t)S(u, t)\, du, \quad \text{(B8)}$$

respectively. In (B8), $P(x, t, t_i)$ explicitly refers to gradient and sinuosity changes.

According to (B1), (B2), and (B4) the structural uplift is given by

$$U(x, t, t_i) = T(x, t) - R(x, t) + B(x_0, t, t_i) - L(x, t, t_i) + P(x, t, t_i). \quad \text{(B9)}$$

The zone of thin-skinned tectonics that we consider in this study extends for only 25 km. Given that the equivalent elastic thickness of the Indian lithosphere is of the order of 80 km [*Lyon-Caen and Molnar*, 1985], lithospheric flexure cannot produce deformation with a wavelength smaller than ~1000 km [e.g., *Turcotte and Schubert*, 1982]. We may therefore assume that the term $L(x, t, t_i)$ does not depend on x along the 25-km-long sections that we are considering. According to (6) we may then replace $B(x_0, t, t_i) - L(x, t, t_i)$ by the sediment accumulation between t and t_i just at front of the MFT, $D(x_0, t, t_i)$, and write

$$U(x, t, t_i) = I(x, t) + D(x_0, t, t_i) + P(x, t, t_i), \quad \text{(B10)}$$

where

$$I(x, t, t_i) = T(x, t, t_i) - R(x, t, t_i) \quad \text{(B11)}$$

is the river incision. Note that neglecting sedimentation and river geometry changes, (B10) equates uplift and incision, as often assumed.

B2. Application to the Bagmati and Bakeya Rivers

The tectonic uplift was computed for the terrace treads T_0, T_1, and T_3 along the Bagmati River according to (B10), assuming no gradient changes and from the paleosinuosities derived from Figure 8a. Figures B2, ED4a and ED4b show the respective contributions to tectonic uplift of river incision, sinuosity changes and base level changes for the three terrace treads. The contribution of river geometry changes become significant at the northern end of the Bagmati canyon where tectonic uplift is not so rapid and because P results from the cumulative effect of geometric changes along a longer river reach.

The tectonic uplift was similarly computed for the terrace treads T_0, T_1, T_2, and T_3 along the Bakeya River from the paleosinuosities derived from Figure 8b. Figures ED5a, ED5b, ED5c, and ED5d show the respective contributions to tectonic uplift of river incision, sinuosity changes, and base level changes. For the terrace T_2 we assume the sinuosity change is intermediate between those of the terraces T_1 and T_3.

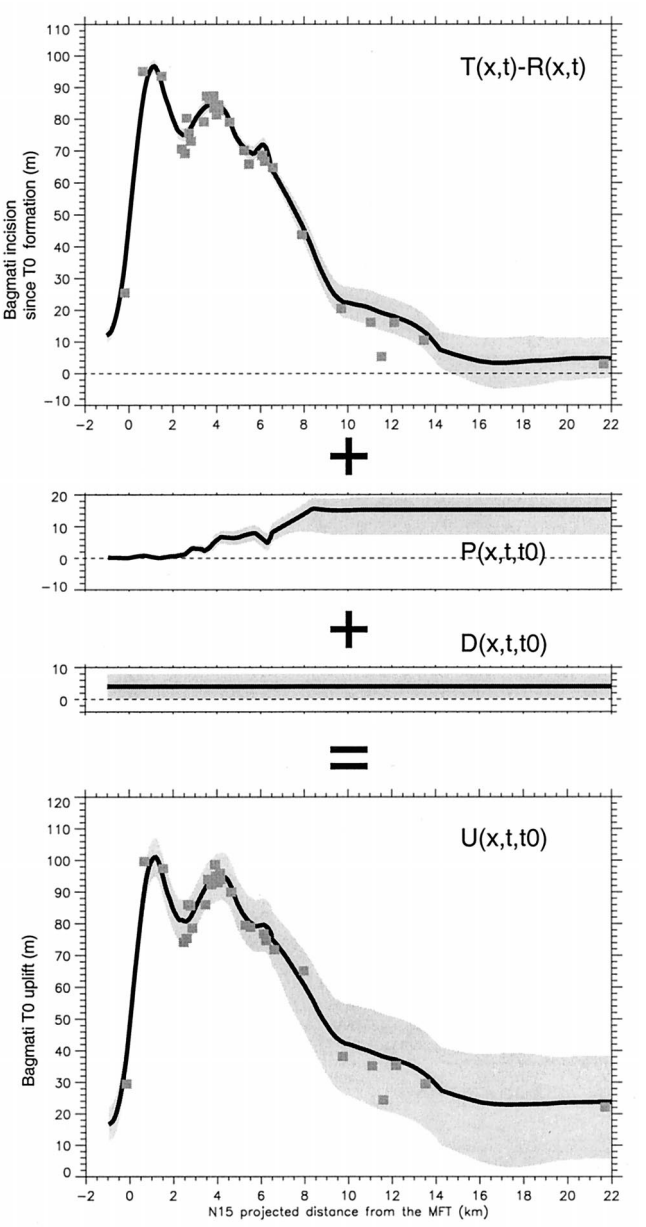

Figure B2. Determination of structural uplift $U(x)$ as a function of incision $T(x) - R(x)$, sinuosity change $P(x)$, and sedimentation in the foreland $D(x)$; from elevation profile of terrace T_0 along the Bagmati River. Field measurements of incision are also shown.

We assume, as for the Bagmati River, that the regional mean gradient of the Bakeya River did not change during the Holocene, assuming an initial knickpoint geometry like that along the modern channel. Given the lack of information on the paleogeometry of the knickpoint, the uncertainty on $P(x, t)$ has been increased and arbitrarily set to a contribution induced by a 50% drop of the knickpoint amplitude.

Finally, it should be observed that the recognition of the role played by base level, gradient, and sinuosity changes induces only small modification of the tectonic uplift pattern. As evident from Figure B2, they essentially contribute to larger un-

certainties. The equations presented in this appendix may therefore be useful in order to test the robustness of the results even if paleosinuosities, paleogradients, and base level changes are poorly constrained.

Appendix C: Computation of Uncertainties

In order to check the estimated uncertainty on measured elevations we computed the standard deviation of the individual measurements z_i from the mean profile $z(x)$:

$$\varepsilon = \sqrt{\sum_{i=1}^{n} [z_p(x_i) - z_i]^2/n}, \tag{C1}$$

where x_i is the distance from the MFT of points P_i, taken normal to the fold strike; z_i is the elevation of that point. If only the field measurements are considered, it yields values, ε^a, between 2 and 4 m, depending on the terrace level. This is consistent with the assigned uncertainties of 3 m (or 5 m for Tomen measurements). When only measurements from the DEM are considered, we get values, $\varepsilon_{\mathrm{DEM}}$, between 7 and 11 m. We may thus have slightly overestimated the uncertainty on elevations measured from the DEM.

The confidence interval on $z(x)$ was computed by considering $z(x)$ as a mean of all the measurements within the sliding window, centered on x, considered as independent variables. One term is related to the uncertainty on the elevations of the top of the terrace. A first term, $\varepsilon_1(x)$, that does not take into account the uncertainty on the gravel thickness, is given by,

$$1/\varepsilon^2(x) = \sum_{x_i^a \in [x-d/2;\, x+d/2]} (1/\varepsilon_i^a)^2 + \sum_{x_j^{\mathrm{DEM}} \in [x-d/2;\, x+d/2]} (1/\varepsilon_j^{\mathrm{DEM}})^2. \tag{C2}$$

We add another term, $\varepsilon_2(x)$, that represents the uncertainty on the thickness of the gravel veneer. We estimate this uncertainty to be 1 m for $x = -2$ km to $x = 14$ km. Farther north we assigned a larger uncertainty of 5 m due to the difficulty of identifying clearly the strath level. The final uncertainty on $z(x)$ is $\varepsilon_z(x) = \varepsilon_1(x) + \varepsilon_2(x)$.

The uncertainty on the incision profile $I(x, t)$ deduced from the elevation profile $z(x)$ of a given strath level that was abandoned at time t is assigned the same uncertainty $\varepsilon_z(x)$, as on $z(x)$. The uncertainty on the elevation of the modern channel is included into the uncertainty on the relative elevation terrace.

The uncertainty on the uplift profile, $U(x, t)$ must account for the uncertainty on

Paleochannel geometry

$$\varepsilon_3(x) = ds/sL(x)S(x) \tag{C3}$$

with $ds/s = 10\%$, obtained after filtering out the small wavelength ($\lambda < 800$ m) of the modern channel and thus considering the induced change of sinuosity.

Base level change

$$\varepsilon_4 = 0.5.t \tag{C4}$$

where t is the age of abandonment of the considered strath terrace. The resulting uncertainty on $U(x, t)$ is then

$$\varepsilon^U(x) = \varepsilon_1(x) + \varepsilon_2(x) + \varepsilon_3(x) + \varepsilon_4. \tag{C5}$$

Appendix D: Determination of the Best Fitting Similarity Ratio Between Two Profiles

Let us consider two profiles $A(x)$ and $B(x)$. $A(x)$ and $B(x)$ may represent the incision or uplift recorded by two different strath levels along a section. We assume that $A(x)$ and $B(x)$ are proportional and look for the most probable value of their ratio k defined by

$$A(x) = kB(x). \tag{D1}$$

Let us now assume that A and B can be written

$$A(x) = A_1(x) + A_2, \tag{D2}$$

$$B(x) = B_1(x) + B_2, \tag{D3}$$

respectively. In the case where A and B represents profiles of uplift, the terms A_2 and B_2 are the contribution of base level changes. If A and B are incision profiles, $A_2 = B_2 = 0$.

Let us assume that uncertainties on A_1, A_2, B_1, and B_2 follow some Gaussian statistics characterized by their respective standard deviation. Let f_{A1}, f_{A2}, f_{B1}, and f_{B2} be the probability laws describing these statistics. If we consider that A_2 and B_2 are known, the probability law for k, associated to values of $A(x)$ and $B(x)$ at a given abscissa x, is

$$f^1_{(x,A_2,B_2)}(k) = \int f_{A_1}(\xi - A_2)\, f_{B_1}\left(\frac{\xi}{k} - B_2\right) \frac{\xi}{k^2}\, d\xi \tag{D4}$$

Let us now consider the probability law on k resulting from the whole profile. The values of A and B at points apart by more than the size, $\lambda = 1$ km, of the filtering window (Appendix A), can be considered to yield independent constraints. We may then write

$$\ln\,(f^2_{(A_2,B_2)}(k)) = \frac{1}{\lambda}\int_0^L \ln\,[f^1_{(x,A_2,B_2)}(k)]\, dx \tag{D5}$$

with L being the length of the profile.

The probability law on k resulting from all possible values of A_2 and B_2 is then

$$f(k) = \int\int f^2_{(\zeta,\chi)}(k)\, f_{A_2}(\zeta)\, f_{B_2}(\chi)\, d\zeta\, d\chi. \tag{D6}$$

The mean value for k and standard deviation is determined from this probability law.

The rms criterion describing the quality of the fit to the data obtained for a given value of k is defined as

$$\mathrm{rms} = \left\{ \left[\sum_{x_i} (A_{T_0}(x_i) - A_T(x_i)/k_{T/T_0})^2/\varepsilon(x_i)^2 \right] \div \left(\sum_{x_i} 1/\varepsilon(x_i)^2 \right) \right\}^{1/2} \tag{D7}$$

where $\varepsilon(x)$ is the standard deviation associated with the Gaussian statistics on $A(x)$ and $B(x)$ (Appendix C).

This procedure is also used to determine the shortening $d(t)$ as a function of dip angles as proposed in the fault bend fold model of terrace deformation. In that case, $A(x)$ is the uplift profile, and $B(x)$ represents the sinus of the dip angle (equation (6)) or corrected dip angle (equation (7) or (10)).

Acknowledgments. We are most grateful to M. R. Pandey, Tandukar and the National Seismological Center (DMG, Kathmandu) for the help in the organization of the field surveys. The Petroleum Project kindly provided access to their seismic profiles. Remote sensing DMG team kindly provided a draft of the sheet covering the surveyed area of the 1:100,000 geological map of Nepal in advance of publication. Francis Guillois and Pascal Benoit have drawn some of the figures. We are indebted to R. Weldon and D. Fisher and to B. Anderson and A. Densmore, who provided thoughtful reviews that led us to significant modifications of the two companion manuscripts that were initially prepared. We are grateful to A. Densmore, D. Granger, and M. Ellis for thoughtful reviews and comments on the present version of the manuscript. We also benefited from comments by Peter Molnar and Paul Tapponnier on an early draft and by Niels Hovius on the modified version.

References

Apotria, T. G., W. T. Suedden, J. H. Spang, and D. V. Wiltschko, Kinematic models of deformation at an oblique ramp, in *Thrust Tectonics*, edited by K. R. McClay, pp. 141–151, Chapman and Hall, New York, 1992.

Appel, E., W. Rösler, and G. Corvinus, Magnetostratigraphy of the Miocene-Pleistocene Surai Khola Siwaliks in west Nepal, *Geophys. J. Int*., *105*, 191–198, 1991.

Armijo, R., P. Tapponnier, J. L. Mercier, and H. Tonglin, Quaternary extension in southern Tibet, *J. Geophys. Res*., *91*, 13,803–13,872, 1986.

Auden, J. B., Transverses in the Himalaya, *Rec. Geol. Surv. India*, *69*, 123–167, 1935.

Bilham, R., K. Larson, J. Freymuller, and Project Idylhim Members, Indo-Asian convergence rates in the Nepal Himalaya, *Nature*, *386*, 61–64, 1997.

Brunel, M., Ductile thrusting in the Himalayas: Shear sense criteria and stretching lineations, *Tectonics*, *5*, 247–265, 1986.

Bull, W., *Geomorphic Response to Climatic Change*, 326 pp., Oxford Univ. Press, 1991.

Burbank, D. W., J. Leland, E. Fielding, R. S. Anderson, N. Brozovic, M. R. Reid, and C. Duncan, Bedrock incision, rock uplift and threshold hillslopes in the northwestern Himalayas, *Nature*, *379*, 505–510, 1996.

Chander, R., Southern limits of major earthquake ruptures along the Himalaya between 15°E and 90°E, *Tectonophysics*, *170*, 115–123, 1989.

Chang, H. H., *Fluvial Processes in River Engineering*, 425 pp., John Wiley, New York, 1988.

Chester, J. S., J. M. Logan, and J. H. Spang, Influence of layering and boundary conditions on fault-bend and fault-propagation folding, *Geol. Soc. Am. Bull*., *103*, 1059–1072, 1991.

Corvinus, G., The Mio-Plio-Pleistocene litho- and biostratigraphy of the Surai Khola Siwaliks in west-Nepal: First results, *C. R. Acad. Sci. Ser. II*, *306*, 1471–1477, 1988.

Cotton, F., M. Campillo, A. Deschamps, and B. K. Rastogi, Rupture history and seismoteictonics of the 1991 Uttarkashi, Himalaya earthquake, *Tectonophysics*, *258*, 35–51, 1996.

Delcaillau, B., *Les Siwaliks de l'Himalaya du Népal Oriental, Fonctionnement et Évolution*, 205 pp., 1992.

Department of Mines and Geology (DMG), Exploration opportunities in Nepal, 33 pp., Kathmandu, Nepal, 1990.

Gansser, A., *Geology of the Himalayas*, Wiley-Interscience, New York, 1964.

Gautam, P., and E. Appel, Magnetic-polarity of Siwalik group sediments of Tinau Khola section in west central Nepal, revisited, *Geophys. J. Int*., *117*, 223–234, 1994.

Gautam, P., B. N. Upreti, and K. Arita, Paleomagnetism and petrochemistry of the Dowar Khola volcanics, central Nepal sub-Himalaya, *J. Nepal Geol. Soc*., *11*, 179–195, 1995.

Harrison, T. M., P. Copeland, S. A. Hall, J. Quade, S. Burner, T. P. Ojha, and W. S. F. Kidd, Isotopic preservation of Himalayan/Tibetan Uplift, denudation, and climatic histories of two molasse deposits, *J. Geol*., *101*, 157–175, 1993.

Hérail, G., and G. Mascle, Les Siwalik du Népal central: Structure et géomorphologie d'un piémont en cours de déformation, *Bull. Assoc. Geogr. Fr*., *471*, 259–267, 1980.

Iwata, S., and T. Nakata, River terraces and crustal movement in the area around Narayanghat, central Nepal, *J. Nepal Geol. Soc*., *5*, 33–42, 1986.

Iwata, S., T. Sharma, and H. Yamanaka, A preliminary report on geomorphology of central Nepal and Himalayan uplift, *J. Nepal Geol. Soc*., *4*, 141–149, 1984.

Jackson, M., and R. Bilham, Constraints on Himalayan deformation inferred from vertical velocity fields in Nepal and Tibet, *J. Geophys. Res*., *99*, 13,897–13,912, 1994.

Jackson, M., S. Barrientos, R. Bilham, D. Kyestha, and Buddhi Shrestha, Uplift in the Nepal Himalaya revealed by spirit leveling, *Geophys. Res. Lett*., *19*, 1539–1542, 1992.

Johnson, G. D., N. M. Johnson, N. D. Opdyke, and R. A. K. Tahirkheli, Magnetic reversal stratigraphy and sedimentary tectonic history of the Upper Siwalik Group, eastern Salt Range and southeastern Kashmir, in *Geodynamics of Pakistan*, edited by A. Farah and K. A. De Jong, pp. 149–165, Geol. Surv. of Pakistan, Quetta, 1979.

Johnson, N. M., N. D. Opdyke, G. D. Johnson, E. H. Lindsay, and R. A. K. Tahirkheli, Magnetic polarity stratigraphy and age of Siwalik Group rocks of the Potwar Plateau, Pakistan, *Palaeogeogr. Palaeoclimatol. Palaeoecol*., *37*, 17–42, 1982.

Karunakaran, C., and A. Ranga Rao, Status of exploration for hydrocarbons in the Himalayan region—Contributions to stratigraphy and structure, Himalayan Geology Seminar, section III, Oil and Natural Gas Resources, *Geol. Surv. India Misc. Publ*., *41*, 1–66, 1979.

Kimura, K., Late quaternary morphotectonics of the Hetauda Dun, Nepal sub-Himalaya, *J. Nepal Geol. Soc*., *11*, 225–235, 1995.

Lavé, J., Tectonique et érosion: L'apport de la dynamique fluviale a l'étude sismotectonique de l'Himalaya du Népal central, these de 3eme cycle, 225 pp., Univ. Paris VII, 1997.

Le Fort, P., Himalayas: The collided range. Present knowledge of the continental arc, *Am. J. Sci*., *275A*, 1–44, 1975.

Le Fort, P., Metamorphism and magmatism during the Himalayan collision, in *Collision Tectonics*, *Geol. Soc. Spec. Publ. London*, *19*, 159–172, 1986.

Leopold, L. B., *A View of the River*, 292 pp., Harvard Univ. Press, 1994.

Lyon-Caen, H., and P. Molnar, Constraints on the structure of the Himalaya from an analysis of gravity anomalies and flexural model of the lithosphere, *J. Geophys. Res*., *88*, 8171–8191, 1983.

Lyon-Caen, H., and P. Molnar, Gravity anomalies, flexure of the Indian plate and the structure, support and evolution of the Himalaya and Ganga Basin, *Tectonics*, *4*, 513–538, 1985.

Mascle, G., and G. Hérail, Les Siwalik: Le prisme d'accrétion tectonique associé à la subduction intracontinentale himalayenne, *Géol. Alpine*, *58*, 95–103, 1982.

Mathur, L. P., and P. Evans, Oil in India, paper presented at International Geological Congress 22nd Session, New Delhi, 1964.

Merritts, D. J., K. R. Vincent, and E. E. Wohl, Long river profiles, tectonism, and eustasy: A guide to interpreting fluvial terraces, *J. Geophys. Res*., *99*, 14,031–14,050, 1994.

Molnar, P., Inversion of profiles of uplift rates for the geometry of dip-slip faults at depth, with examples from the Alps and the Himalaya, *Ann. Geophys*., *5*, 663–670, 1987.

Molnar, P., and Q. Deng, Faulting associated with large earthquakes and the average rate of deformation in central and eastern Asia, *J. Geophys. Res*., *89*, 6203–6227, 1984.

Molnar, P., and P. Tapponnier, Cenozoic tectonics of Asia: Effects of a continental collision, *Science*, *189*, 419–426, 1975.

Molnar, P., E. T. Thorson, B. C. Burchfield, Q. Deng, X. Feng, J. Li, G. M. Raisbeck, Shi Jianbang, Z. Wu, F. Yiou, and H. You, Quaternary climate change and the formation of river terraces across growing anticlines on the north flank of the Tien Shan, China, *J. Geol*., *102*, 583–602, 1994.

Mugnier, J. L., G. Mascle, and T. Faucher, La structure des Siwaliks de l'Ouest Nepal: Un prisme d'accrétion intracontinental, *Bull. Soc. Geol. Fr*., *163*(5), 585–595, 1992.

Nakata, T., Geomorphic history and crustal movements of the foothills of the Himalayas, *Sci. Rep. 22*, 177 pp., Tohoku Univ., Geogr. Dept., 1972.

Nakata, T., Active faults of the Himalaya of India and Nepal, *Spec. Pap. Geol. Soc. Am*., *232*, 243–264, 1989.

Ni, J., and M. Barazangi, Seismotectonics of the Himalayan collision zone: Geometry of the underthusting Indian plate beneath the Himalaya, *J. Geophys. Res*., *89*, 1147–1163, 1984.

Pandey, M. R., and P. Molnar, The distribution of intensity of the Bihar-Nepal earthquake of 15 January 1934 and bounds on the extent of the rupture zone, *J. Geol. Soc. Nepal*, *5*, 22–44, 1988.

Pandey, M. R., R. P. Tandukar, J. P. Avouac, J. Lavé, and J. P. Massot,

Interseismic strain accumulation on the Himalayan crustal ramp (Nepal), *Geophys. Res. Lett*., *22*, 751–754, 1995.

Patriat, P., and J. Achache, India-Eurasia collision chronology has implications for crustal shortening and driving mechanisms of plates, *Nature*, *311*, 615–621, 1984.

Pearson, G. W., B. Becker, and F. Qua, High precision ^{14}C measurements from German and Irish oaks to show the natural ^{14}C variations from 7890 to 5000 BC, *Radiocarbon*, *35*, 93–104, 1993.

Personius, S. F., Late Quaternary stream incision and uplift in the forearc of the Cascadia subduction zone, western Oregon, *J. Geophys. Res*., *100*, 20,193–20,210, 1995.

Pilgrim, G. E., Preliminary note on a revised classification of the tertiary fresh water deposits of India, *Rec. Geol. Surv. India*, *40*, 185–205, 1910.

Pilgrim, G. E., The correlation of the Siwalik with mammal horizons of Europe, *Rec. Geol. Surv. India*, *42*, 264–326, 1913.

Pilgrim, G. E., Preliminary note on some recent mammalian collection from the basal beds of Siwalik, *Rec. Geol. Surv. India*, *48*, 98–101, 1917.

Ratschbacher, L., W. Frisch, G. Liu, and C. Chen, Distributed deformation in southern and eastern Tibet during and after the India-Asia collision, *J. Geophys. Res*., *99*, 19,917–19,946, 1994.

Rockwell, T. K., E. A. Keller, M. N. Clark, and D. L. Johnson, Chronology and rates of faulting of Ventura River terraces, California, *Geol. Soc. Am. Bull*., *95*, 1466–1474, 1984.

Sastri, V. V., An overview of petroleum geotectonis of the region to the north and south of the Himalaya, Himalayan Geology seminar, section III, Oil and Natural Gas resources, *Geol. Surv. India Misc. Publ*., *41*, 247–276, 1979.

Sastri, V. V., L. L. Bhandari, A. T. R. Raju, and A. K. Datta, Tectonic framework and subsurface stratigraphy of the Ganga basin, *J. Geol. Soc. India*, *12*, 222–233, 1971.

Schelling, D., A balanced cross-section through the eastern Nepal Siwaliks Hills, Bagmati River region: Implications for the structure of the southern Himalaya, *J. Nepal Geol. Soc*., *8*, 1–10, 1992a.

Schelling, D., The tectonostratigraphy and structure of the eastern Nepal Himalaya, *Tectonics*, *11*, 925–943, 1992b.

Schelling, D., and K. Arita, Thrust tectonics, crustal shortening and the structure of the Far-Eastern Nepal Himalaya, *Tectonics*, *10*, 851–862, 1991.

Seeber, L., and J. Armbuster, Great detachment earthquakes along the Himalayan arc and the long term forecasts, in *Earthquake Prediction: An International Review*, *Maurice Ewing Ser*., vol. 4, edited by D. W. Simpson and P. G. Richards, pp. 259–277, AGU, Washington, D. C., 1981.

Seeber, L., and V. Gornitz, River profiles along the Himalayan arc as indicators of active tectonics, *Tectonophysics*, *92*, 335–367, 1983.

Seidl, M. A., and W. E. Dietrich, The problem of channel erosion into bedrock, *Catena Suppl*., *23*, 101–124, 1992.

Stöcklin, J., Geology of Nepal and its regional frame, *J. Geol. Soc. London*, *137*, 1–34, 1980.

Stuiver, M., and B. Becker, High precision decadal calibration of the radiocarbon time scale, AD 1950–6000 BC, *Radiocarbon*, *35*, 35–65, 1993.

Suppe, J., Geometry and kinematics of fault bend folding, *Am. J. Sci*., *283*, 684–721, 1983.

Tokuoka, T., K. Takayasu, M. Yoshida, and K. Hisatomi, The Churia (Siwalik) group of the Arung Khola area, west central Nepal, *Mem. Fac. Sci. Shimane Univ*., *20*, 135–210, 1986.

Turcotte, D., and G. Schubert, *Applications of Continuum Physics to Geological Problems*, 450 pp., John Wiley, New York, 1982.

Weldon, R. J., Late Cenozoic geology of Cajon Pass: Implications for tectonics and sedimentation along the San Andreas fault, Ph.D. thesis, 400 pp., Calif. Inst. of Technol., Pasadena, 1986.

Yang, C. T., and C. C. S. Song, Theory of minimum rate of energy dissipation, *J. Hydraul. Div. Am. Soc. Civ. Eng*., *105*(HY7), 769–784, 1979.

Yeats, R., and R. J. Lillie, Contemporary tectonics of the Himalayan frontal fault system: Folds, blind thrusts and the 1905 Kangra earthquake, *J. Struct. Geol*., *13*, 215–225, 1991.

Zhao, W., K. D. Nelson, and Project INDEPTH Team, Deep seismic reflection evidence for continental underthrusting beneath southern Tibet, *Nature*, *366*, 557–559, 1993.

J. P. Avouac, Laboratoire de Géophysique, CEA, 91680, Bruyères-Le-Châtel, France. (avouac@ldg.bruyeres.cea.fr)

J. Lavé, Laboratoire de Géodynamique des Chaînes Alpines, BP 53, F-38041 Grenoble, France. (jlave@ujf-grenoble.fr)

(Received December 1, 1998; revised June 14, 1999;
accepted August 20, 1999.)